SYNTHETIC ACOUSTIC LOGS OVER BED BOUNDARIES AND HORIZONTAL FISSURES

by

R.A. Stephen

P.O. Box 567
West Falmouth, MA 02574

ABSTRACT

The finite difference method is used to predict the effects of wave propagation in boreholes with vertically varying elastic properties. Specifically horizontal interfaces between rock types (for example shales and sandstones) and between rock and horizontal liquid fissures of varying width are considered.

The amplitudes of the transmitted compressional head waves and Stoneley waves are only slightly affected by thin horizontal fissures and stringers. On the other hand, the pseudo-Rayleigh wave, when it is present (e.g., in sandstones), can be almost totally blocked by a very thin (1 cm) horizontal fissure. Both compressional head waves and pseudo-Rayleigh waves show significant reflections at horizontal discontinuities. Stoneley waves and PL modes are not significantly reflected.

In general, mode conversion is not a significant effect in the bed boundary and horizontal fissure models considered. Although some very strong effects can be observed on the transmitted and reflected waves none of the models showed significant scattering (for example, from pseudo-Rayleigh waves to compressional head waves).

The effects observed at bed boundaries in the field (for example, Paternoster and Larrère, 1985) are adequately simulated by the synthetics. Adjusting for the differences in offsets of the two cases, arrival times and amplitudes correspond well. The only exception to this is the absence of identifiable mode conversions. Larger offset models will be necessary to clearly distinguish any mode conversions that may be occurring.

INTRODUCTION

Wave propagation in vertically homogeneous cylindrical boreholes has been studied theoretically by a number of investigators (Biot, 1952; White, 1962; White and Zechman, 1968; Tsang and Rader, 1979; Cheng and Toksöz,1981; Schoenberg et al., 1981; Paillet and White, 1982; Baker, 1984; Tubman et al., 1984; Schmitt and Bouchon,1985). However many features of field logs cannot be predicted by these vertically homogeneous

more energy is available to propagate back into the well as a head wave.

A Sandstone-Shale Contact

The appearance of the full waveform log changes dramatically on crossing the contact from a sandstone to a shale(Figure 3). The head wave velocity (the inverse of the slope of the first arrival) changes sharply at the contact but there is little change in head wave amplitude and coherency is maintained. The pseudo-Rayleigh wave on the other hand is almost totally eliminated at the contact. There are weak reflections of the pseudo-Rayleigh and compressional waves as readily observed on the residual log. In fact in this case the residual log is necessary to see the reflected compressional wave. On the original log the reflection is masked by downgoing pseudo-Rayleigh and Stoneley waves which are large amplitude. The Stoneley wave continues on almost unaffected below the contact.

These observations seem reasonable because the pseudo-Rayleigh and compressional waves are being "supported" by the rigidity of the rock. The pseudo-Rayleigh wave depends heavily on "total internal reflection". There is no total internal reflection in the shale case since energy can always leak into shear waves (shear velocity is less than the fluid velocity). The Stoneley wave is essentially a fluid-borne wave modified slightly by the properties of the hole wall.

A Shale-Sandstone Contact

Similar effects are seen when the waves traverse from a shale to a sandstone. In this case the compressional head wave velocity increases and amplitudes are enhanced. The only noticeable reflection on the residual log is the compressional head wave. The pseudo-Rayleigh wave was not present in the original shale log and hence has nothing to reflect. As in the previous case the Stoneley wave propagates past the contact almost unaffected. A weak reflection of the Stoneley wave can be observed in this example because the pseudo-Rayleigh wave is not present to mask it. It is interesting to note that although the original shale log had strong PL mode amplitudes the reflected PL modes are very weak. It would be very difficult to identify a shale-sandstone contact based on reflected waves!

A Thin Horizontal Fissure

In this example a very thin (0.75 cm) horizontal fissure, filled with mud, is introduced into the sandstone model (Figure 5). Strong reflections are observed for both the compressional head wave and the pseudo-Rayleigh wave packet. The residual log has a

very symmetrical appearance suggesting a reflection coefficient for this example of 0.5. This strong reflection of both phases is surprising since the crack is much thinner than a wavelength. The wavelength in the water is about 10 cm, over ten times the crack width, and the wavelength in the solid is about 40 cm. Further examples of horizontal mud filled fissures will be discussed later (Figures 17–21).

Shale Stringers in a Sandstone

The effects of shale stringers are not as dramatic as the mud-filled fissures. Figures 6 and 7 show synthetic logs for stringers 15 cm and 3 cm wide respectively. The 15 cm wide stringer is wide enough to show the change in slope of the compressional wave arrival over the interval. As for the sandstone-shale example (Figure 3) the compressional wave amplitude is affected very little by the contacts. There is a weak reflection of the compressional head wave at the upper boundary but any reflections of this wave by the lower boundary are masked by larger amplitude pseudo-Rayleigh waves (see the residual log, Figure 6c). The pseudo-Rayleigh amplitudes are weak in the shale region and strengthen again in the sandstone on the far side of the stringer. Weak, but clear, reflections of the pseudo-Rayleigh wave are generated at both the upper and lower edges of the stringer.

In the case of the stringer three centimeters wide, there appears to be no serious disruption in the propagation of the compressional, pseudo-Rayleigh, and Stoneley paths. The weak reflections of the pseudo-Rayleigh and compressional waves are similar to the sandstone-shale contact example in Figure 3.

Sandstone Stringers in a Shale

Similar effects are seen in the case of a sandstone stringer in shale. For the 15 cm wide stringer (Figure 8) the apparent velocity of the compressional head wave increases over the interval of the stringer. Once past the stringer the Stoneley waves regain their coherence. Weak reflections of the compressional head wave can also be seen from both upper and lower contacts. When the width of the stringer is reduced to 3 cm (Figure 9) the pattern is similar to the shale-sandstone contact (Figure 4) except that the guided waves regain their coherency below the stringer.

Flushed and Damaged Sandstone Examples

The next series of synthetic logs demonstrates the effects of flushed and damaged sandstones adjacent to the well. Again as a reference we show the vertically homogeneous

models for 4.5 cm wide altered zones of flushed sandstone and damaged sandstone in Figures 10 and 11 respectively.

When a flushed section of sandstone terminates within a sandstone layer (Figure 12) the resultant logs are indistinguishable from the totally flushed case (Figure 10). Note the very weak amplitudes of the pseudo-Rayleigh waves in the residual log. Similarly when the flushed zone terminates at a shale (Figure 13) the logs are indistinguishable from the sandstone-shale contact case (Figure 3).

The effects of damaged sandstone zones terminating at sandstones or shales (Figures 14 and 15 respectively) also are quite similar to their undamaged counterparts (Figures 1 and 3). In the case of the damaged sandstone zone terminating at a sandstone there are essentially no reflections, but the transmitted compressional waves and pseudo-Rayleigh waves have slight changes in amplitude and/or phase (Figure 14c). This effect is more noticeable for the terminating damaged sandstone than for the terminating flushed sandstone (Figure 12c). When the damaged sandstone terminates at a shale the general picture of reflected and transmitted waves is the same as for undamaged sandstone terminating at a shale (Figure 3) but the amplitudes vary up to 6 db.

For the frequencies and hole widths considered here it is reasonable to conclude that flushed and damaged zones do not appreciably effect the logs. Note that these conclusions are also model dependent. Stephen (1985) and Stephen et al. (1985) proposed that damaged zones could be represented by continuous velocity gradients. In this case the appearance of the logs in the presence of the damaged zone is remarkably altered due to loss of the pseudo-Rayleigh wave. If the gradient model were used for the damaged and flushed zones above we would expect more dramatic differences in the vicinity of the horizontal contacts. The validity of the models for damaged and flushed zones (gradients versus homogeneous layers) will depend on comparisons with real data. The finite difference code can handle each model equally well.

Horizontal Fissures of Varying Thicknesses

The next series of models shows the effects of varying fissure thickness on the logs. They differ from the models above (which were based on Bhasavanija, 1983) in hole radius, mud properties, and depth of propagation in the well. Figure 16 again sets the stage by showing results for a vertically homogeneous sandstone. The compressional head wave, PL modes, pseudo-Rayleigh wave, and Stoneley wave can be identified. Figures 17, 18, 19 and 20 then show the effects of horizontal fissures as the thickness varies from 1cm to 10, 20 and 80 cm. Residual logs were not prepared for this series.

The only noticeable reflection is the pseudo-Rayleigh wave which has essentially the same amplitude for all crack widths. The transmitted pseudo-Rayleigh wave is also very strongly attenuated below the uppermost sandstone-mud contact.The particle motions

of the pseudo-Rayleigh wave in the formation are almost purely horizontal (see Figures 7c and 7d, in Stephen et al., 1985). Consequently even a relatively thin (a tenth of a wavelength or less) horizontal crack with zero shear strength can decouple the pseudo-Rayleigh wave from the lower formation. Thin cracks are apparently just as effective as thick cracks in this process.

Stoneley waves are transmitted, with attenuation of less than 6 db, past cracks up to 10 cm thick. Thicker cracks attenuate the Stoneley wave very strongly but there is no noticeable Stoneley wave reflection. In keeping with the concept of the Stoneley wave being a mud-borne phenomenon, the energy travels down the wellbore and radiates into the crack. For crack widths less than about a wavelength the Stoneley wave becomes reguided again below the crack. For larger crack widths the energy diffuses out into the crack. It is apparent that the amplitude of the Stoneley wave decreases and its attenuation increases with the width of the crack. This can obviously be related to the permeability of the crack. This result is qualitatively similar to observed data (Paillet, 1980) and the theoretical model of Mathieu and Toksöz (1984).

Compressional head waves are probably reflected at the cracks as in Figure 3 but cannot be observed because of interference with larger amplitude PL and pseudo-Rayleigh waves. The transmitted compressional waves are weaker by about 6 db for all crack widths than in the absence of the crack but are not as strongly attenuated as the Stoneley waves in the 20 and 80 cm model.

Shale Stringers of Various Thickness in a Sandstone

The next series of logs (Figures 21–24) demonstrates the effects of shale stringers of various widths(1, 10, 20, 80 cm respectively). Oddly enough the pseudo-Rayleigh wave is reflected from even thin shale stringers almost as effectively as from thin fissures. The pseudo-Rayleigh wave propagates past thin stringers (less than a wavelength) with about 6 db of attenuation. For shale stringers of greater width the pseudo-Rayleigh wave is almost totally eliminated.

The Stoneley wave is less effected by the shale stringers. For stringers 10 cm or less it is unaffected but for larger stringers it is attenuated by about 6 db.

The compressional head wave exhibits similar behavior to the above case for horizontal fissures.

A Suite of Logs over a Sandstone-Shale Contact

The above examples all represent the response at a vertical distribution of pressure receivers to a single source in the vicinity of various horizontal contacts. An actual

log however consists of a sequence of traces all obtained at a constant source-receiver offset but for different depths relative to the contact(an iso-offset section). The next sequence of figures demonstrates the synthesis of an iso-offset section. Because the source to contact distance differs for an iso-offset section the finite difference code must be run for each source depth. Since this is time consuming and expensive, results are not routinely shown in this format.

Figure 25 shows the usual format log for a vertically homogeneous sandstone model with a slightly lower frequency and formation shear velocity than the previous sandstone models. The changes were made in order to enhance the Stoneley wave amplitudes. (For vertically homogeneous models the single shot format is equivalent to the iso-offset section.) Figure 26 shows the single shot format for the reflection from a sandstone-shale contact. The general pattern of reflections and transmissions is similar to the sandstone-shale example of Figure 3. The reflected compressional wave amplitudes are slightly higher for this model and the reflected pseudo-Rayleigh wave is less coherent.

The iso-offset section for the sandstone-shale contact is presented in Figure 7. The source-receiver offset has been fixed at 75 cm and the tool has been moved past the contact at 15 cm intervals. It is difficult to identify the presence of the contact on the unmodified log (Figure 27a). While the tool is above the contact, the traces are identical indicating no significant response due to reflections. As the source and receiver span the contact, slight delays in compressional wave travel time are observed, the head wave and pseudo-Rayleigh wave amplitudes are attenuated slightly, and the PL modes are essentially eliminated. The Stoneley wave is unaffected.

However, on the residual iso-offset section the compressional head wave and pseudo-Rayleigh wave reflections can be identified and could be used to identify the location of the contact. This is the only indication of the "chevron" pattern observed in full waveform logs such as EVA and attributed to fissures or contacts (Paternoster and Larrère, 1985). The effects of the bed boundaries are less evident in the synthetic logs than in the observed EVA data because the data were collected over a larger offset and the phases were more separated. The reflected events for example were not as rapidly masked by later large amplitude arrivals. The fan filtering used in Paternoster and Larrère (1985) could also be used on the synthetic data to enhance scattered arrivals rather than using the residual logs. Despite the considerable difference in source-receiver offsets, a cursory comparison of the synthetic and observed data indicates similar magnitudes for the reflected and transmitted events at bed boundaries.

CONCLUSIONS

The finite difference method is a suitable technique for studying the effects of horizontal bed boundaries and fissures on full waveform acoustic logs. Sharp solid-solid and liquid-solid contacts which vary in two dimensions can be stably and accurately handled.

The amplitudes of the transmitted compressional head waves and Stoneley waves are only slightly affected by thin horizontal fissures and stringers. On the other hand, the pseudo-Rayleigh wave, when it is present (e.g., in sandstones), can be almost totally blocked by a very thin (1 cm) horizontal fissure. Both compressional head waves and pseudo-Rayleigh waves show significant reflections at horizontal discontinuities. Stoneley waves and PL modes are not significantly reflected.

In general, mode conversion is not a significant effect in the bed boundary and horizontal fissure models considered. Although some very strong effects can be observed on the transmitted and reflected waves none of the models showed significant scattering (for example, from pseudo-Rayleigh waves to compressional head waves).

The effects observed at bed boundaries in the field (for example, Paternoster and Larrère, 1985) are adequately simulated by the synthetics. Adjusting for the differences in offsets of the two cases, arrival times and amplitudes correspond well. The only exception to this is the absence of identifiable mode conversions. Larger offset models will be necessary to clearly distinguish any mode conversions that may be occurring.

ACKNOWLEDGEMENTS

This work was supported by the Full Waveform Acoustic Logging Consortium at M.I.T.

REFERENCES

Alterman, Z., and Loewenthal,D., 1972, Computer generated seismograms; in Methods in Computational Physics, 12; Bolt, B.A., Ed., Academic Press Inc., 35-164.

Baker, L.J., 1984, The effect of the invaded zone on full wave train acoustic logging; Geophysics 49, 796-809.

Bhasavanija, K. 1983, A finite difference model of an acoustic logging tool: the borehole in a horizontally layered geologic medium; Ph.D. Thesis, Colorado School of Mines, Golden, Colorado.

Biot, M.A., 1952, Propagation of elastic waves in a cylindrical bore containing fluid; J.Appl.Phys., 23, 997-1005.

Cheng, C.H., and Toksöz, M.N., 1981, Elastic wave propagation in a fluid filled borehole and synthetic acoustic logs; Geophysics, 46, 1042-1053.

Mathieu, F., and Toksöz, M.N., 1984, Determination of fracture permeability using

acoustic logs; S.A.I.D. Ninth Int. Formation Evaluation Trans., Paper 47.

Nicoletis, L.,1981, Simulation numerique de la propagation d'ondes sismiques dans les milieux stratifies a deux et trois dimensions; contribution a la construction et a l'interpretation des sismogrammes synthetiques; Ph.D. Thesis, L'universite Pierre et Marie Curie, Paris VI.

Paillet, F.L., 1980, Acoustic propagation in the vicinity of fractures which intersect a fluid-filled borehole; Trans. 21st SPWLA Ann. Logging Symp., Paper DD.

Paillet, F.L., and White, J.E., 1982, Acoustic modes of propagation in a borehole and their relationship to rock properties; Geophysics, 47, 1215-1228.

Pardo-Casas, F., Cheng, C.H., and Stephen, R.A., 1984, The study of wave propagation in a borehole using the finite difference method; M.I.T. Full Waveform Acoustic Logging Consortium Annual Report, 1984.

Paternoster, B., and Larrère, M., 1985. Effects of layer boundaries on FWAL and dip estimation (oblique events); M.I.T. Full Waveform Acoustic Logging Consortium Annual Report, 1985.

Schmitt, D.P., and Bouchon, M., 1985, Full-wave acoustic logging: synthetic microseismograms and frequency-wavenumber analysis; Geophysics, 50, 1756-1778.

Schoenberg, M., Marzetta, T., Aron, J., and Porter, R., 1981, Space-time dependence of acoustic waves in a borehole; J. Acoust. Soc. Am., 70, 1496-1507.

Stephen, R.A., 1983, A comparison of finite difference and reflectivity seismograms for marine models; Geophys. J. R. Astr. Soc., 72, 39-58.

Stephen, R.A., 1985, Finite difference synthetic acoustic logs for boreholes with sharp, rough interfaces; M.I.T. Full Waveform Acoustic Logging Consortium Annual Report, 1985.

Stephen, R.A., Pardo-Casas, F., and Cheng, C.H., 1983. Finite difference synthetic acoustic logs; M.I.T. Full Waveform Acoustic Logging Consortium Annual Report, 1983.

Stephen, R.A., Pardo-Casas, F., and Cheng, C.H., 1985, Finite-difference synthetic acoustic logs; Geophysics, 50, 1588-1609.

Tsang, L., and Rader, D., 1979, Numerical evaluation of the transient acoustic waveform due to a point source in a fluid-filled borehole; Geophysics, 44, 1706-1720.

Tubman, K.M., Cheng, C.H., and Toksöz, M.N., 1984, Synthetic full-waveform acoustic

logs in cased boreholes; Geophysics, 49, 1051-1059.

White, J.E., 1962, Elastic waves along a cylindrical bore; Geophysics, 27, 327-333.

White, J.E., and Zechman, R.E., 1968, Computed response of an acoustic logging tool; Geophysics, 33, 302-310.

APPENDIX A: SOURCE AND BOUNDARY CONDITIONS FOR A RIGID TOOL

Bhasavanija (1983) and Pardo-Casas et al. (1984) discuss finite difference methods for introducing a rigid tool in the center of a fluid-filled borehole with a distributed source. Neither method is satisfactory. The limitations will be discussed here and a third more acceptable approach presented.

Bhasavanija (1983) introduces a distributed source of horizontal displacements for a short length (9-10 grid points) along the wall of the rigid tool. None of the source points has any component of vertical displacement. It can be shown that the horizontal and vertical displacements independently satisfy scalar wave equations for a fluid. (Take the elastic wave equation in terms of dispacement,set the shear modulus equal to zero, and apply the irrotational property of fluids, $\nabla \times u = du/dz - dw/dx = 0$, to the cross derivative terms.) Since the source motion is purely horizontal, only horizontal particle motions will propagate through the fluid. This is a violation of the irrotational property of fluids and is physically unrealistic. Consequently it is questionable whether any of the resulting seismograms in Bhasavanija (1983) are physically meaningful.

Pardo-Casas et al. (1984) tried to remedy the situation by applying a boundary condition formulation for liquid-solid interfaces along the borehole wall and thus computing values for vertical displacement in the fluid using the same horizontal displacements as Bhasavanija (1983). Whether correct or not, this formulation is very cumbersome and is unnecessary.

In order to guarantee (to an acceptable approximation) irrotational particle motions in the fluid it is sufficient to make every point in the distributed source a compressional point source. This can be easily done in the source formulation of Alterman and Loewenthal (1972) and Stephen (1983) where the source is introduced along the edges of a rectangular box (for example, 5 grid points wide by 12 grid points long) about the source. The effect of a distribution of point compressional sources (for example, 10 grid points long) along the wall of the tool can be computed by superposition at the edges of the box. Physically realistic horizontal and vertical displacements in the liquid are then propagated into the well bore.

Figure A-1 shows synthetic logs for the sandstone model of Figure 4-1 in Bhasavanija

(1983). We used the code of Pardo-Casas et al. (1984) but introduced the source as a weighted distribution of compressional point sources rather than horizontal displacements. The weighting in depth and the time dependence of the source was the same as Bhasavanija (1983). The compressional and shear head wave arrivals are quite similar in the two figures. However there are quite significant differences in the pseudo-Rayleigh and Stoneley wave groups. We attribute these differences to the different source formulations used in the two codes. Since the horizontal displacement source of Bhasavanija (1983) is physically incorrect, we prefer Figure A-1 as a representation of the actual wave field.

The boundary formulations at the rigid tool-fluid interface used by Bhasavanija (1983) and Pardo-Casas et al. (1984) are also more complicated than necessary. In Bhasavanija (1983) a fictitious line is introduced into the tool, the wave equation is used along the tool wall, and the displacements on the fictitious line are determined from the irrotational property of fluids. The validity of this approach is accidental since the irrotational property would not be expected to hold continuously across the tool wall. There is some justification for the approach of Bhasavanija (1983) since the top and bottom end of the tool are included. However the major conclusions of the rigid, finite-length tool analysis were that mode conversion was negligible and that tube wave reflections from the top and bottom of the tool arrived after the geologically significant energy.

The approach of Pardo-Casas et al. (1984) is based on a second order finite difference approximation for a liquid-solid interface given by Stephen et al. (1983) and is even more complicated. Although this additional complexity yields more accurate results for real solids it is unnecessary for perfectly rigid solids.

A simpler scheme than either Bhasavanija (1983) or Pardo-Casas et al. (1984) is as follows. The horizontal (normal) displacement is continuous across the tool wall and is zero since the tool is rigid. The horizontal derivative of the vertical displacement in the fluid is also zero since it equals the vertical derivative of the horizontal displacement (the condition for irrotation, $du/dz - dw/dx = 0$). These conditions are equivalent to a vertical axis of symmetry (Stephen, 1983 and Stephen et al., 1983). To allow for the radius of the tool, the correct radius for points away from the tool wall can simply be introduced to the finite difference formulation for the wave equation. There is a small complication in this case for the source since it is still being generated using a zero radius assumption. Since the source is being introduced into the grid over a very small region (much less than a wavelength) this complication is unlikely to be important and the results should correspond to the correct solution for a cylindrical (annular) compressional source.

Figures A-2 and A-3 compare two representations for the model parameters used in Figure 1 of the main text. Figure A-2 corresponds to a point source on the axis of symmetry of a borehole with a radius of 6 cm. The code here is the same as outlined in Stephen et al. (1983) and uses the second order boundary condition formulation for

the fluid-formation contact. Figure A-3 corresponds to a distribution of point sources at the axis of symmetry (as in Figure A-1 but with a 15 kHz source instead of 12 kHz). The radius from the source to the formation is still 6 cm but the radii used in the finite difference calculations are increased everywhere by 7 cm. to approximate a rigid tool with a radius of 7 cm. The formulation for the fluid-formation boundary is the same as Figure A-2. Figure A-3 is a better attempt at representing the effects of a rigid tool than Figure A-2 but is somewhat more complicated.

In the rigid tool case the compressional head wave is much larger than the PL modes (Figure A-3b). In the open hole case the compressional head wave and PL modes have about the same amplitude (Figure A2-b). The guided wave packet is slightly broader and has larger amplitudes later in the wave train for the distributed source (Figure A-3). A better analysis of the guided waves could be carried out in the frequency-wavenumber domain (see Appendix B).

In summary, to represent a rigid tool in the finite difference grid assume that the wall of the tool is coincident with the left hand edge which is an axis of symmetry. The radius of the borehole wall in the model corresponds to the thickness of the annulus around the tool in the real situation. The range terms in the finite difference formulation for the wave equations should be modified to correspond to the range from the center of the tool in the real situation. The field corresponding to either a single compressional point source or a distribution of compressional point sources, located at the vertical axis of symmetry, can be introduced along the edges of the source box.

APPENDIX B: FINITE DIFFERENCE SYNTHETIC ACOUSTIC LOGS PORTRAYED IN THE FREQUENCY-WAVENUMBER DOMAIN

Schmitt and Bouchon (1985) have shown that the frequency-wavenumber domain shows properties of the wavefield in the borehole which cannot easily be determined from the time-space domain. Probably the most useful property is the separation of the "guided wave packet" into its constituent modes, pseudo-Rayleigh and Stoneley waves. The corresponding phase velocities and relative energy content as a function of frequency, for each wave type can be identified.

In the case of Schmitt and Bouchon (1985) the frequency-wavenumber results are an intermediate step in the computation of their "discrete wavenumber" acoustic logs. Our finite difference synthetic acoustic logs are computed in time and space but frequency-wavenumber results can be obtained by taking a two dimensional Fourier transform. In this case the frequency-wavenumber results will correspond more closely to the results one would expect by transforming actual log data. The effects of adequately sampling the borehole array data in space and time and of the location of the array in the borehole can be directly observed. Also since the finite difference method can be used to study

vertical heterogeneities in the well the frequency-wavenumber domain can potentially be used to further determine the properties of the reflected, transmitted and scattered phases.

Tests were carried out to check the value of looking at acoustic logs in the frequency-wavenumber domain. We chose the vertically homogeneous sandstone model (Figure 16). However for the transform studies the pressure receivers were located on the axis of the well, between 1.6 and 3.0 m below the source, at a separation of 4 cm (36 depth samples). The time series ran from 0.0 to 2.5 msecs at a sampling rate of 0.008 msecs (312 time samples). The Nyquist frequency is 62.5 kHz and the Nyquist wavenumber is 12.5 (1/m). The source has a peak frequency of 15.0 kHz with lower and upper half power frequencies of 10.2 and 20.4 kHz.The data used in the transform are shown in Figure B-1. The compressional head wave, PL modes, pseudo-Rayleigh, and Stoneley waves can be readily identified.

In order to transform the data with a two dimensional Fast Fourier Transform (FFT) algorithm the time series were padded with zeroes out to 512 samples and the depths were padded with null traces out to 64 traces. Gibb's phenomenon effects (ringing and acausal arrivals) associated with sharp transitions in the time and depth series were reduced by applying cosine tapers within 20 points of the beginning and end of the time series and within 10 traces of the beginning and end of the depth series.

Figure B-2 shows a section of the frequency-wavenumber domain. Figure B-2a is the real part of the transformed field and Figure B-2b is the power spectrum. At least at these gains the real part, which contains phase information, has better resolution than the power spectrum. More wave types can be identified. These representations are not as full of wave types as the results of Schmitt and Bouchon (1985) (see their Figure 2 for a radius of 0.cm for a hard formation) because our source is band limited (about 10 to 20 kHz) and the receivers span only a limited aperture of the borehole (1.6 to 3.0 m). The dominant energy lies between 12 and 24 kHz indicating that for receivers at this depth low frequency energy has been preferentially lost into the formation.

The predominant arrival is the pseudo-Rayleigh wave which for our configuration consists primarily of the PR1 mode. The peak energy of the mode has a phase velocity of 2.3 km/s corresponding to the formation shear velocity. As outlined in Cheng and Toksöz (1981) the pseudo-Rayleigh wave is dispersive, consisting of phase velocities ranging from the formation shear velocity to the borehole fluid velocity. In our example this corresponds to the energy to the left of the 2.3 km/s line.

The energy to the right of the 2.3 km/s line is the associated resonance of the borehole (Schmitt and Bouchon, 1985). Since this falls between the formation compressional and shear wave phase velocities it can be identified as leaky modes, PL modes, or compressional head wave multiples (Stephen et al., 1985). The disruption between the resonances and the pseudo-Rayleigh waves at the formation shear wave phase velocity, which is described in Schmitt and Bouchon (1985), is not observed in our results.

A small amplitude shear head wave arrival, which is non-dispersive, is observed at higher frequencies and wavenumbers than the pseudo-Rayleigh wave.

Figure B-3 shows a section of the frequency-wavenumber plot which is closer to the origin and at a higher amplitude than Figure B-2. The pseudo-Rayleigh wave is still the largest feature and appears at the formation shear wave phase velocity. A weak Stoneley wave can be observed at lower frequencies. It is slightly dispersive with phase velocities ranging between the borehole fluid velocity (1.8 km/s) and the tube wave velocity. (Biot, 1952, discusses the Stoneley wave behavior for a similar model to ours. For a formation shear velocity to borehole fluid velocity of 1.5, a Poisson's ratio in the solid of 0.25, and a density ratio of 0.5 the tube wave velocity is about 0.9 of the borehole fluid velocity. In our case the tube wave velocity is about 1.6 km/s.)

The region between the formation compressional and shear wave phase velocities shows the leaky mode energy which melds into the pseudo-Rayleigh wave at the shear velocity line.

Two borehole resonances can be observed to the left of the formation compressional velocity line. The lowest frequency resonance is associated with PR2, which can be observed faintly. The higher frequency resonance seems to stand alone.

There is no clear observation of the compressional head wave in either Figure B-2 or B-3. The compressional head wave velocity could possibly be inferred from the location of the resonances but it would not be well resolved.

In conclusion, the frequency-wavenumber representation of the finite difference synthetic acoustic log is useful in separating the various components of the guided wave packet. Because of the band limited nature of the source and the limited aperture of the receiver array the frequency-wavenumber representation of observed data is not as complete as the result of Schmitt and Bouchon (1985). The Stoneley wave arrival, the pseudo-Rayleigh modes, and the borehole resonances are easier to identify in the frequency-wavenumber domain than the time-depth domain. The compressional and shear head wave arrivals and the PL modes are easier to identify in the time-depth domain.

This preliminary investigation of the two dimensional transform of a finite difference synthetic acoustic log is encouraging. Similar analysis should be carried out on models containing horizontal bed boundaries and fissures to gain further insight into the reflection and transmission of the guided wave packet.

TABLE 1. ELASTIC PROPERTIES AND DENSITIES FOR THE MATERIALS USED IN THIS PAPER

MATERIAL	V_p (km/sec)	V_s (km/sec)	ρ (g/cm^3)
MUD	1.65	0.00	1.50
MUD1	1.80	0.00	1.20
SHALE	2.40	1.40	2.10
SHALE1	2.00	1.15	1.60
SANDSTONE	4.00	2.30	2.30
FLUSHED SANDSTONE	4.13	2.27	2.37
DAMAGED SANDSTONE	3.63	2.18	2.37
SANDSTONE1	4.00	2.00	2.30

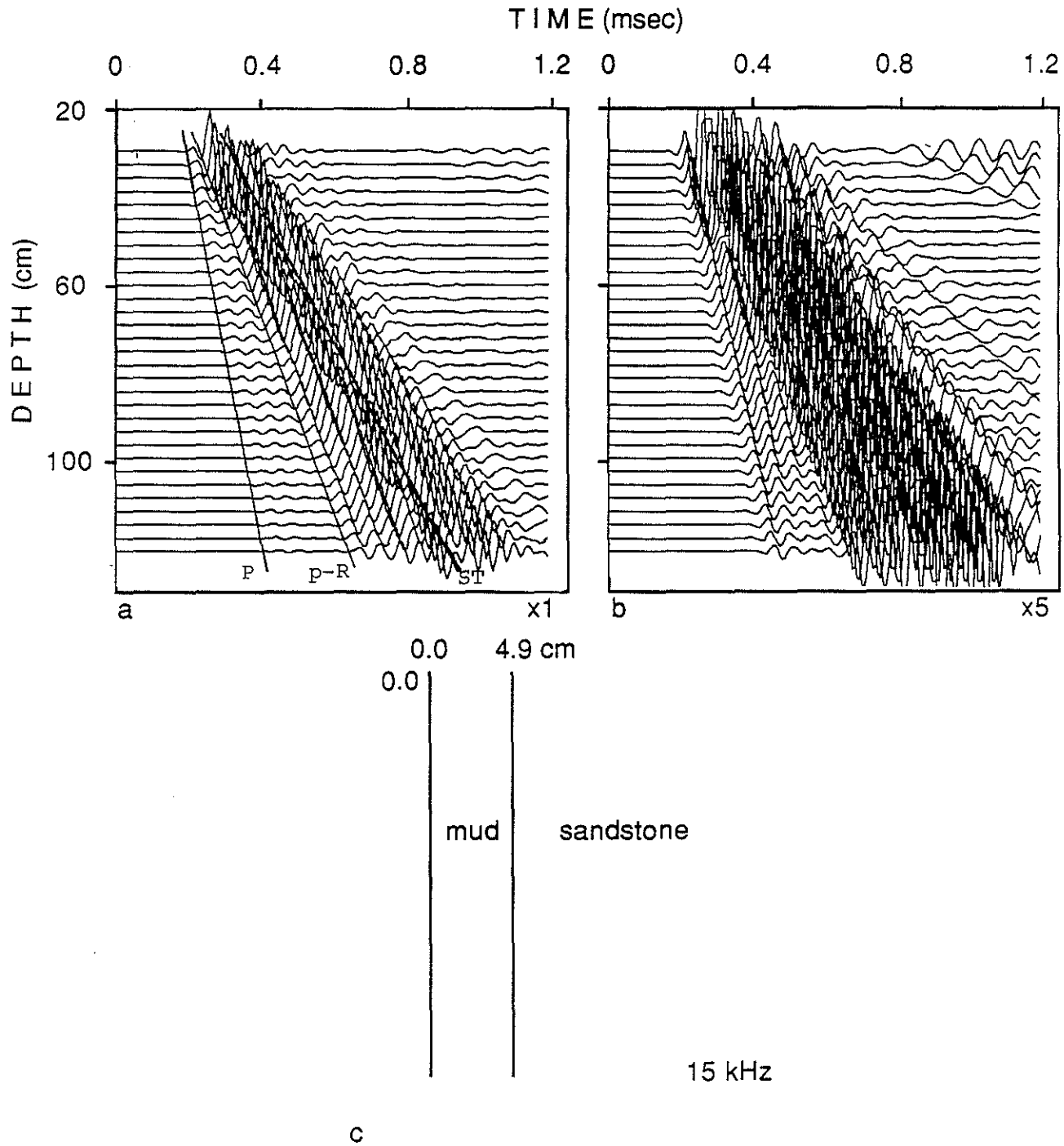

Figure 1: Synthetic full waveform acoustic log for a vertically homogeneous sandstone. The compressional, pseudo-Rayleigh and Stoneley waves can be identified on the figure. In all subsequent figures the borehole geometry, peak source frequency and formation are identified on the figure. The parameters corresponding to the formation names are given in Table 1. All plots correspond to pressure observed at the axis of symmetry. In Figures 1 – 15 a) is unity gain and b) is five times unity gain.

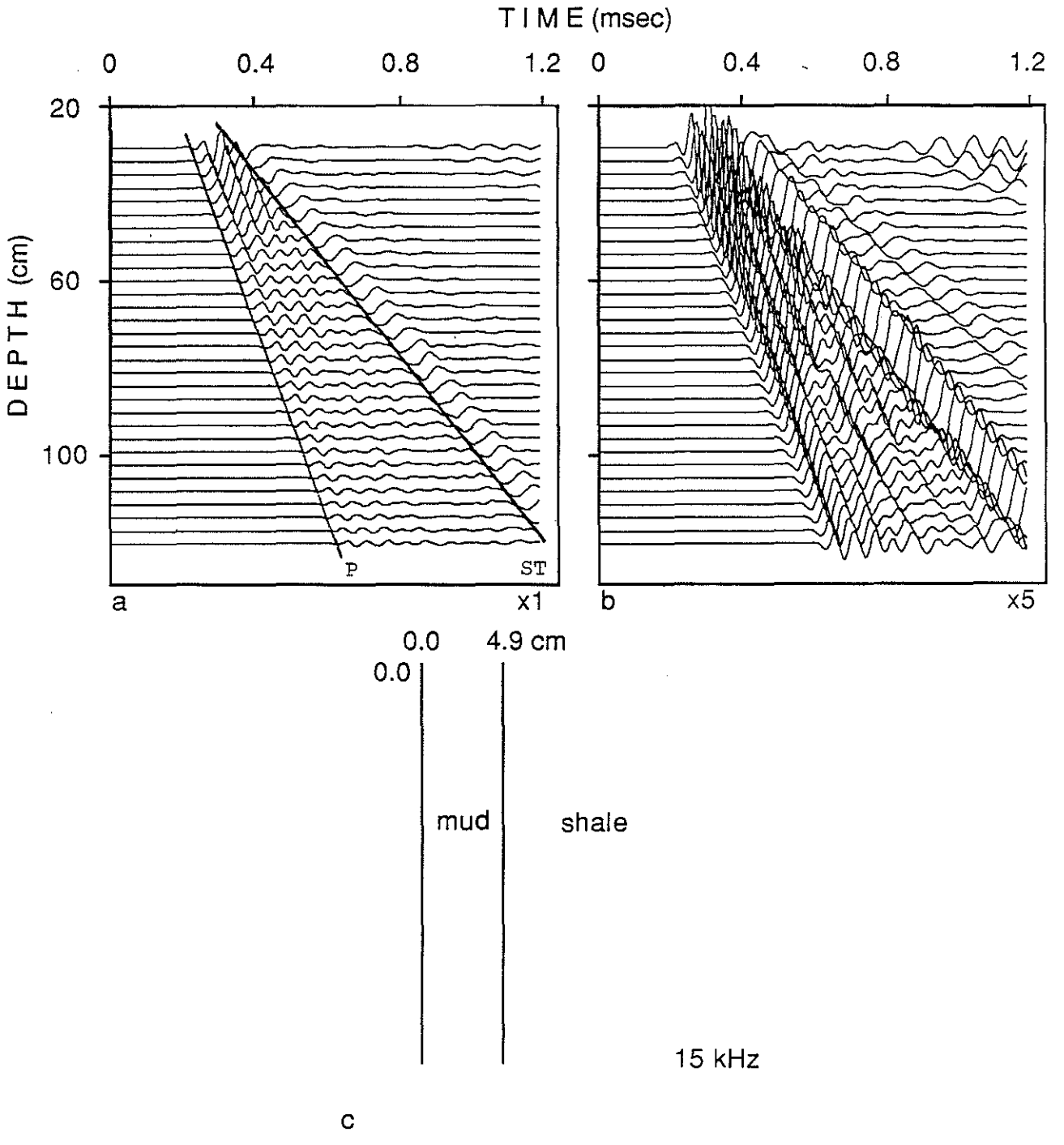

Figure 2: Synthetic full waveform acoustic log for a vertically homogeneous shale. Note the absence of the pseudo-Rayleigh wave and the larger amplitude PL mode in comparison with the sandstone model (Figure 1).

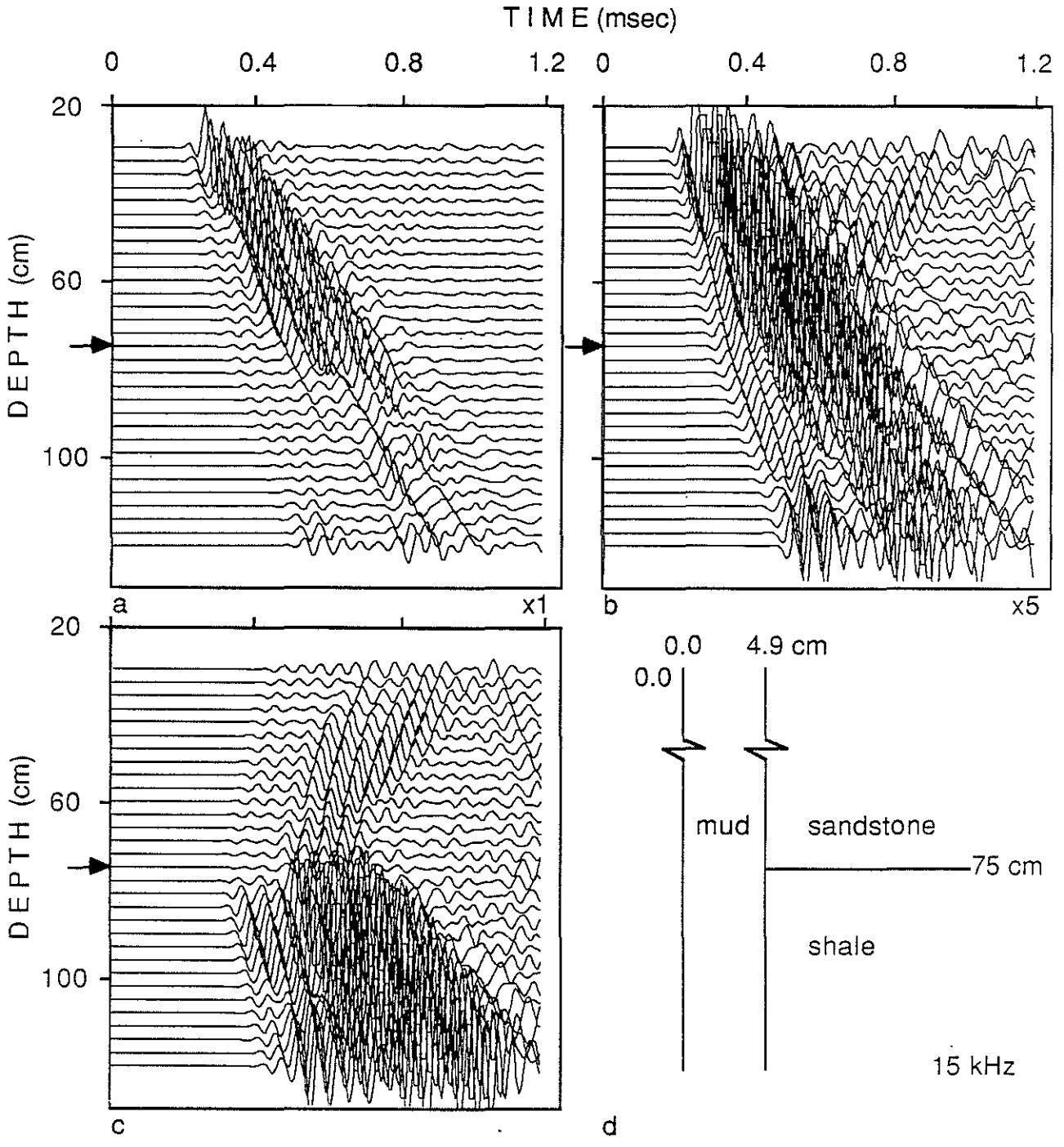

Figure 3: Synthetic full waveform acoustic log for a sandstone-shale contact. Figure c is the residual log, which is the difference between the log with the vertical heterogeneity and the corresponding homogeneous log. Note the strong reflections of the compressional head wave and pseudo-Rayleigh waves.

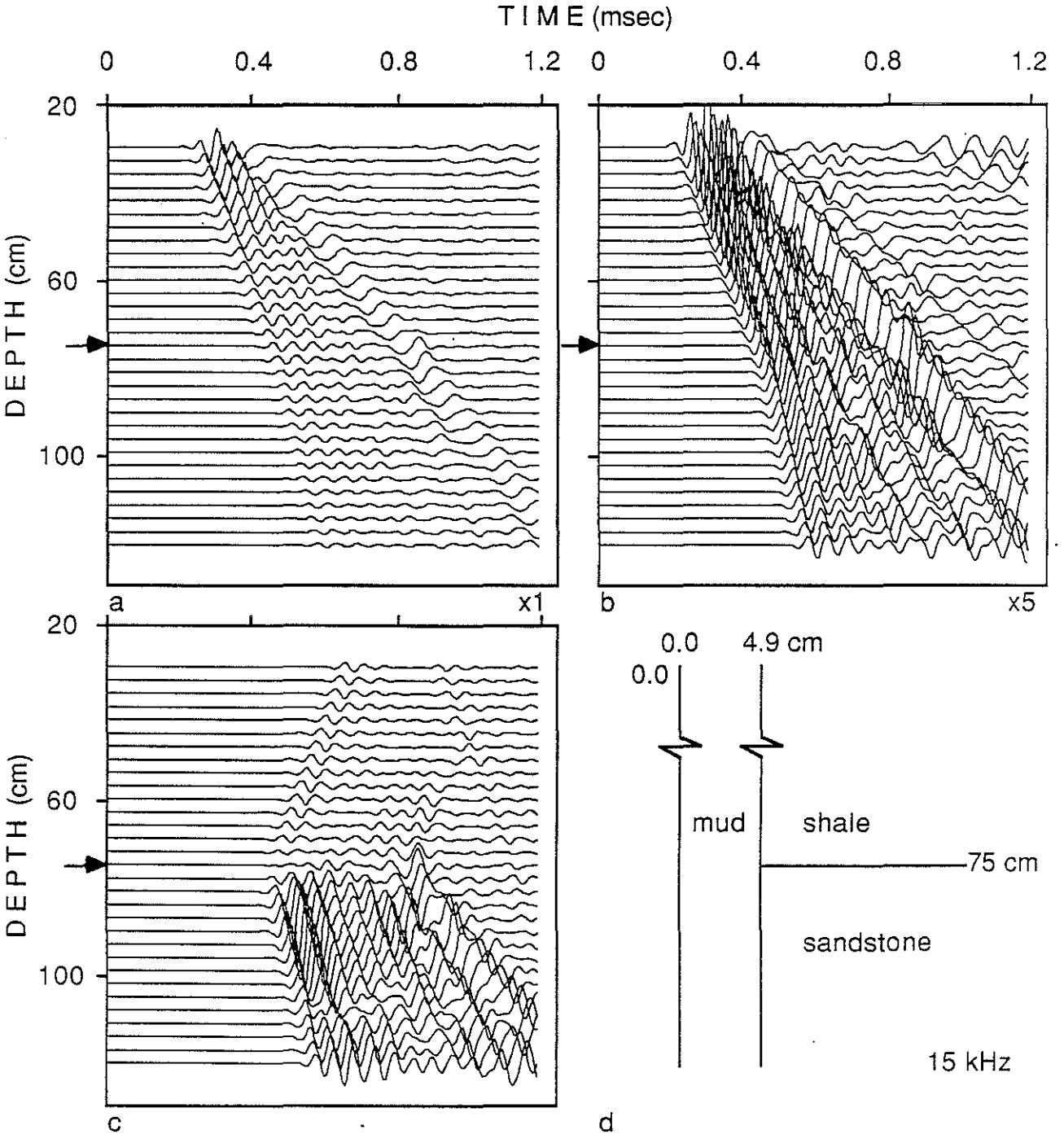

Figure 4: Synthetic full waveform acoustic log for a shale-sandstone contact. Only the compressional head wave is significantly reflected.

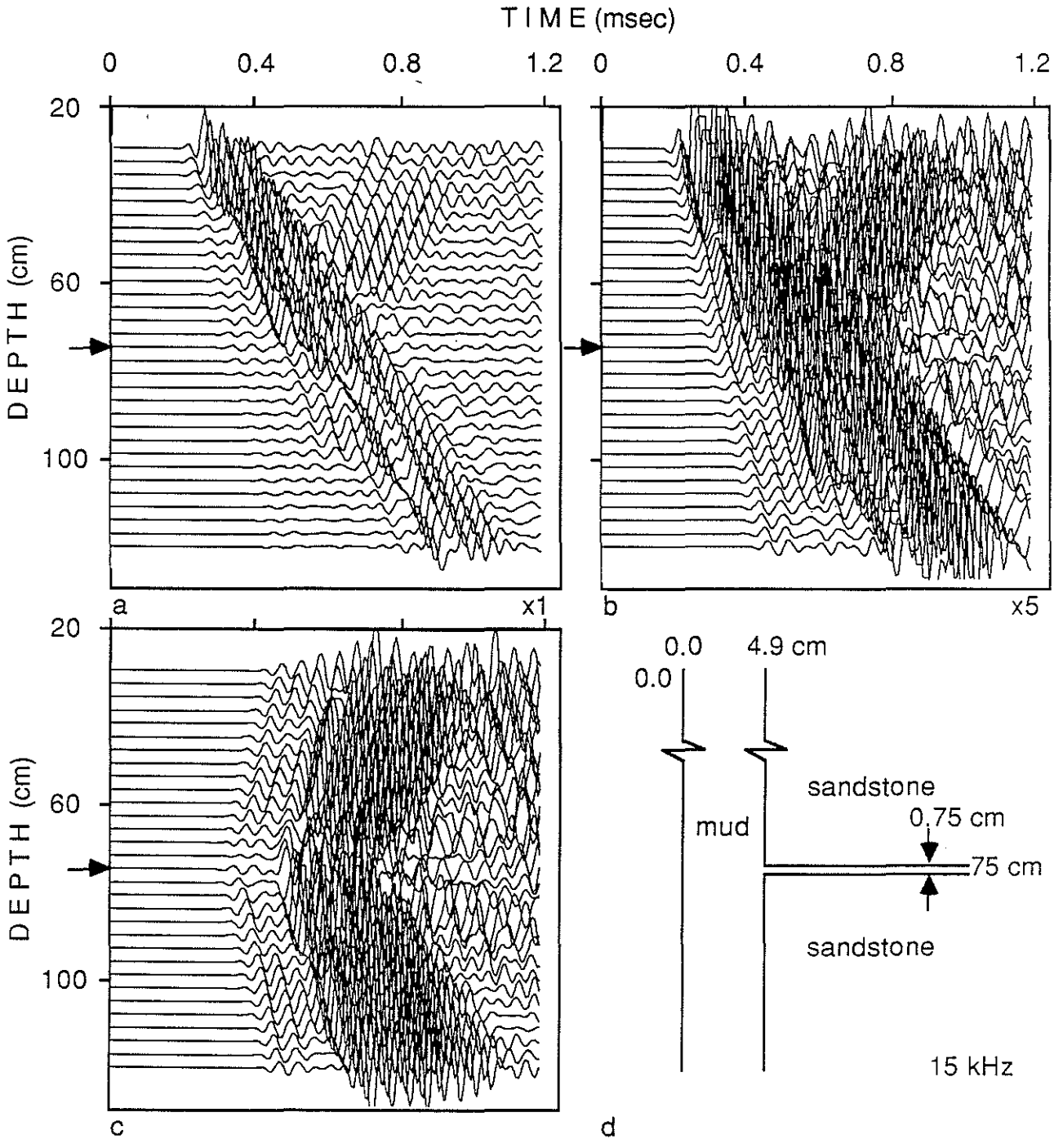

Figure 5: Synthetic full waveform acoustic log for a 0.75 cm thick horizontal fissure in a sandstone. Note the very strong reflections from this very thin fissure.

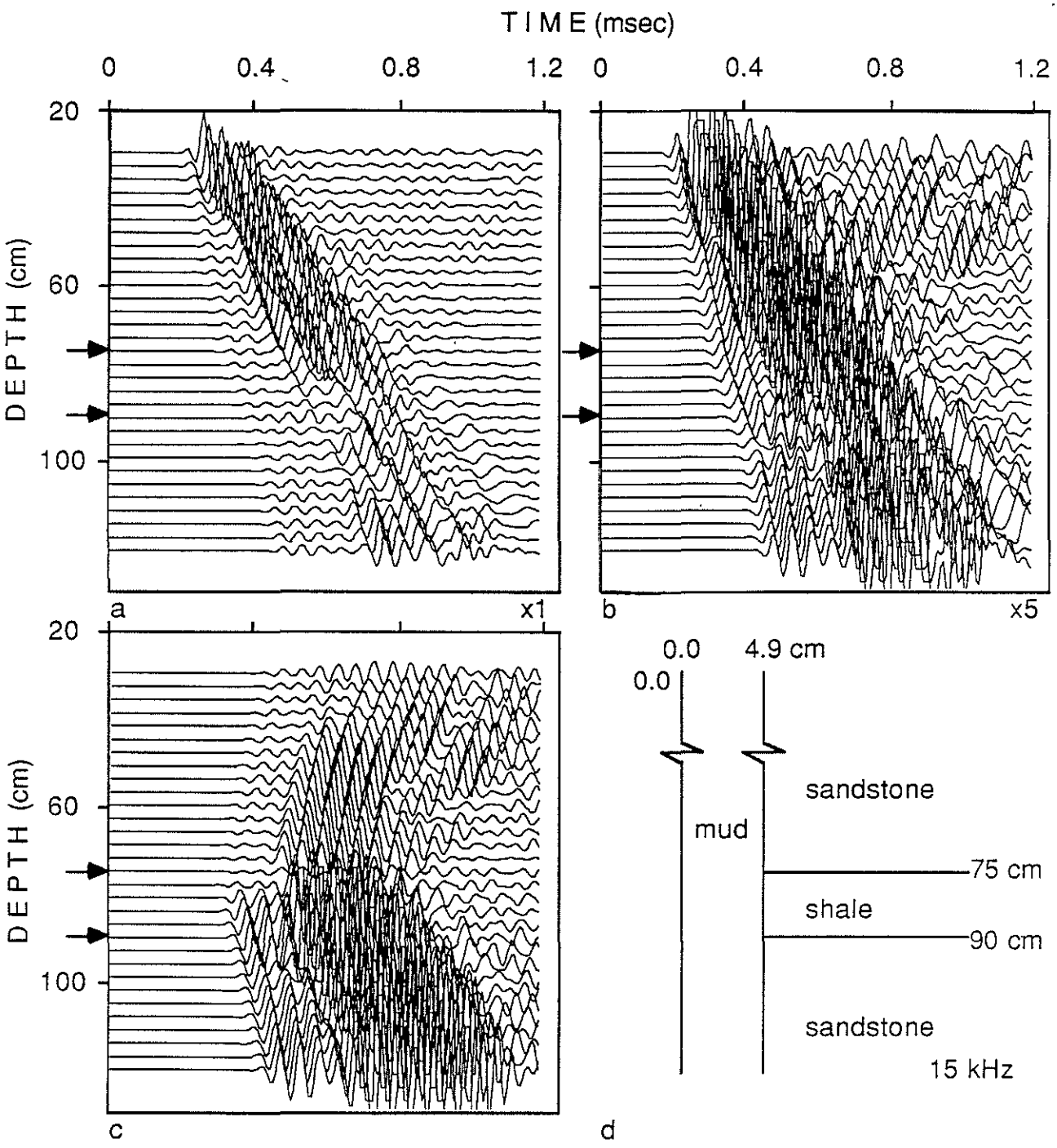

Figure 6: Synthetic full waveform acoustic log for a 15 cm thick shale stringer in a sandstone.

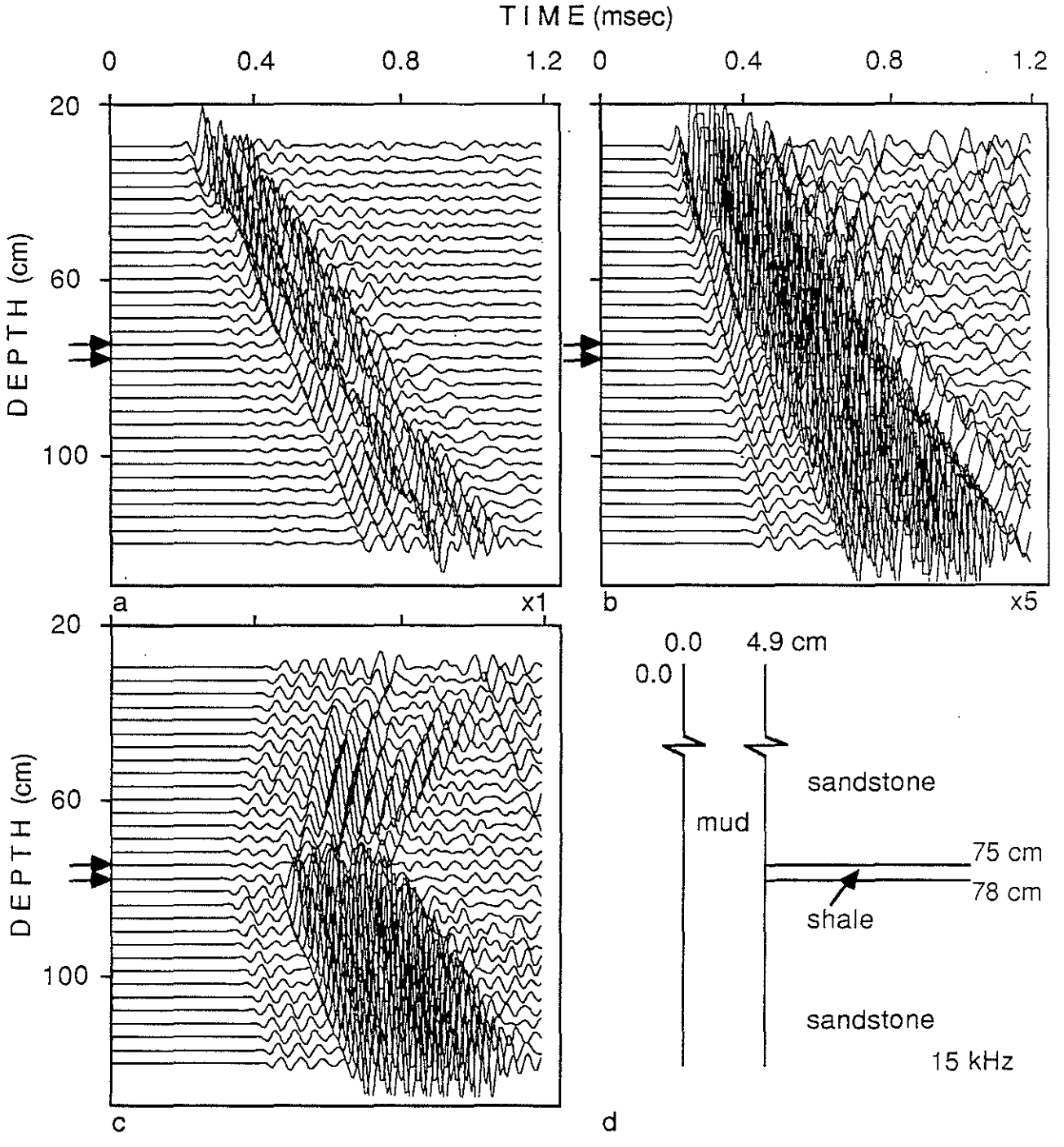

Figure 7: Synthetic full waveform acoustic log for a 3 cm thick shale stringer in a sandstone.

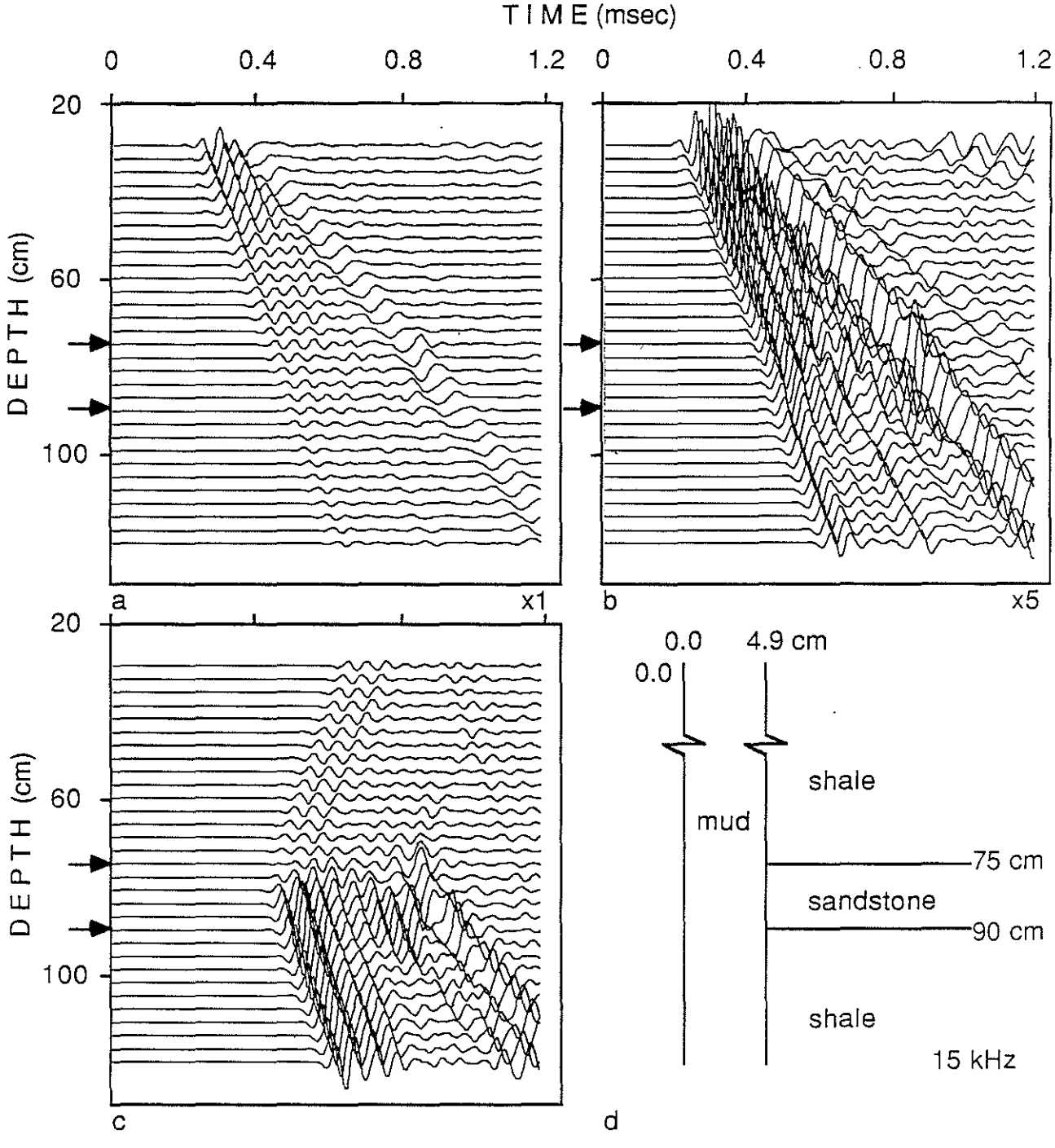

Figure 8: Synthetic full waveform acoustic log for a 15 cm thick sandstone stringer in a shale.

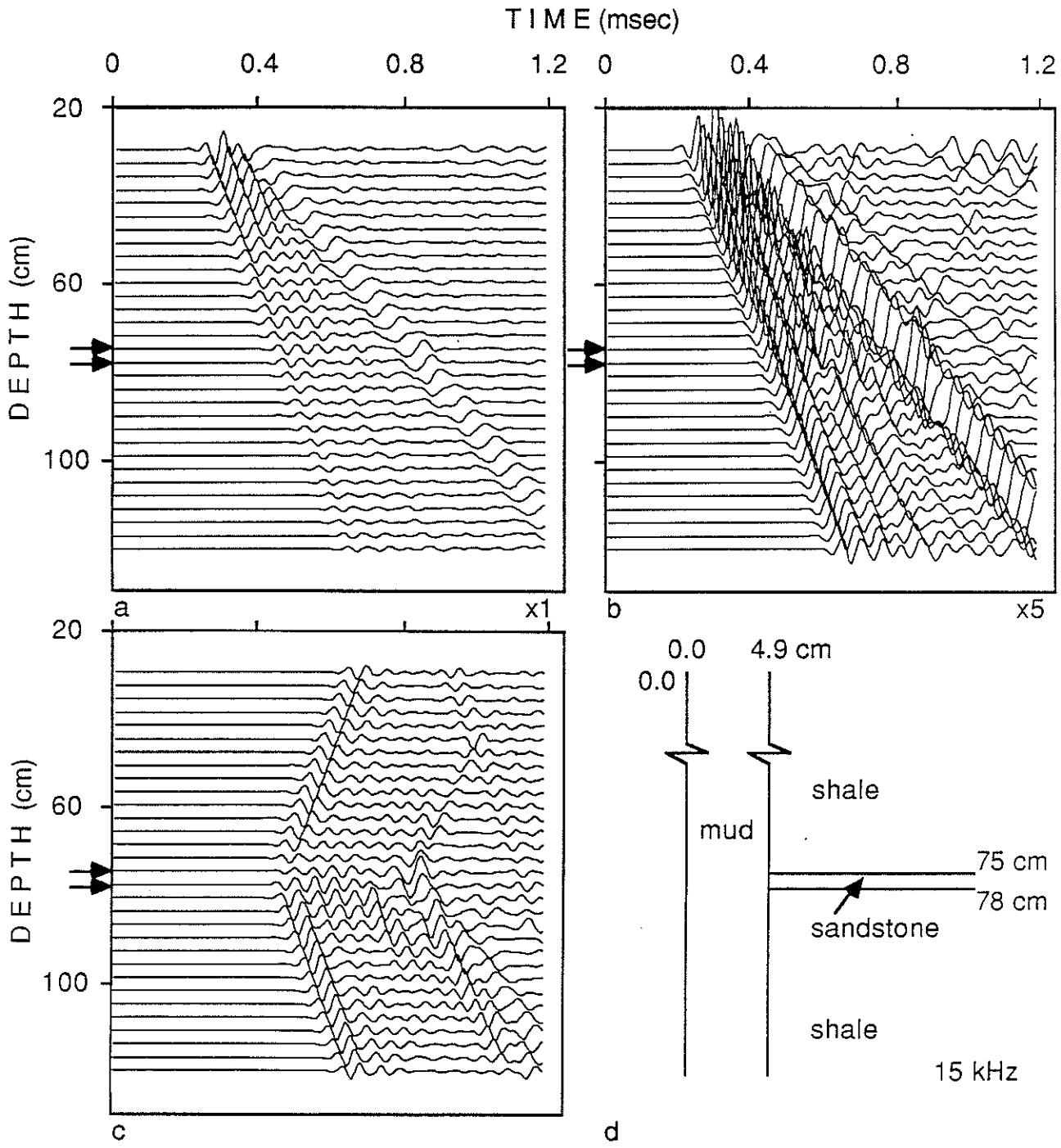

Figure 9: Synthetic full waveform acoustic log for a 3 cm thick sandstone stringer in a shale.

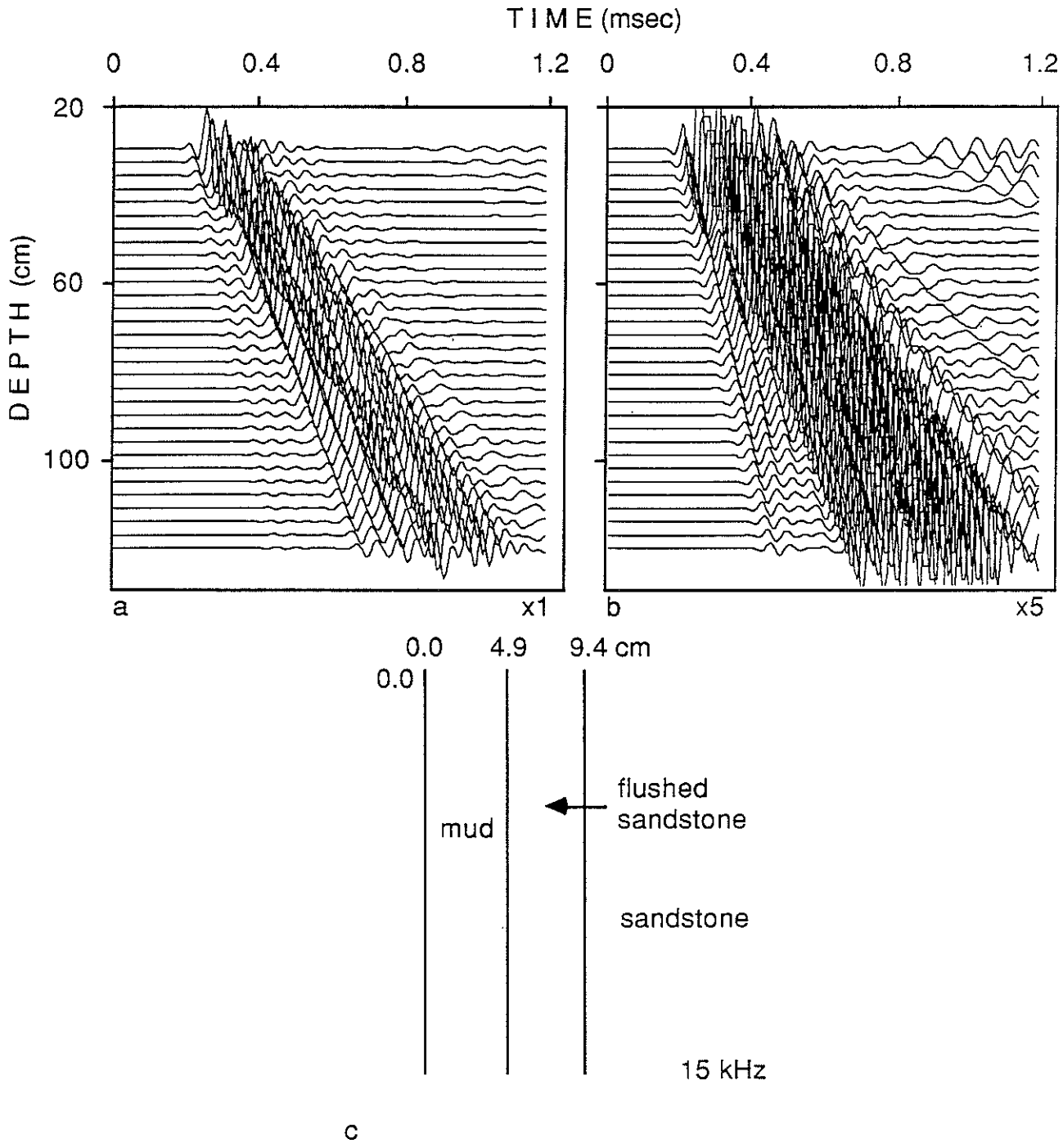

Figure 10: Synthetic full waveform acoustic log for a vertically homogeneous sandstone model with a flushed zone adjacent to the hole.

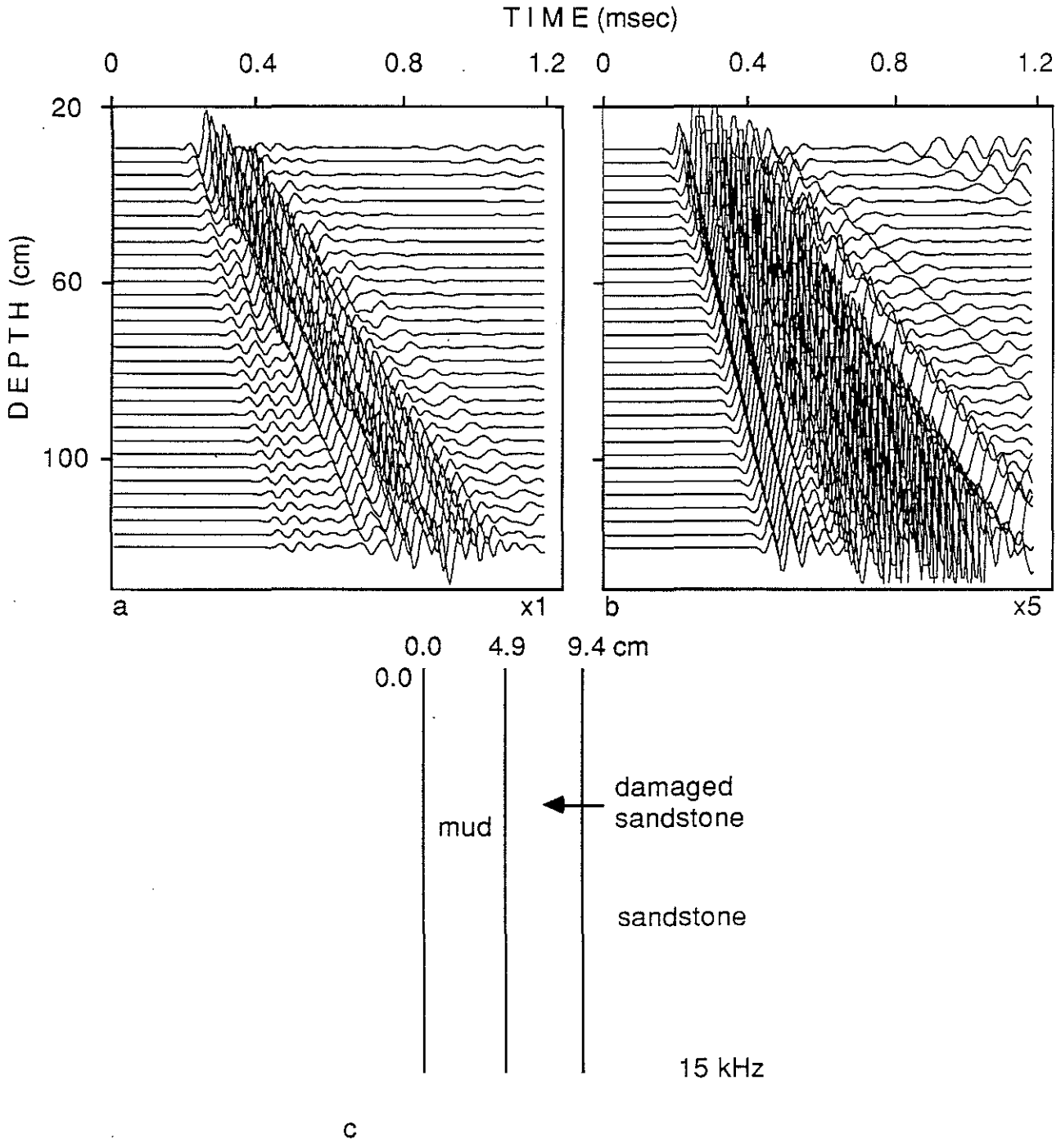

Figure 11: Synthetic full waveform acoustic log for a vertically homogeneous sandstone model with a damaged zone adjacent to the hole.

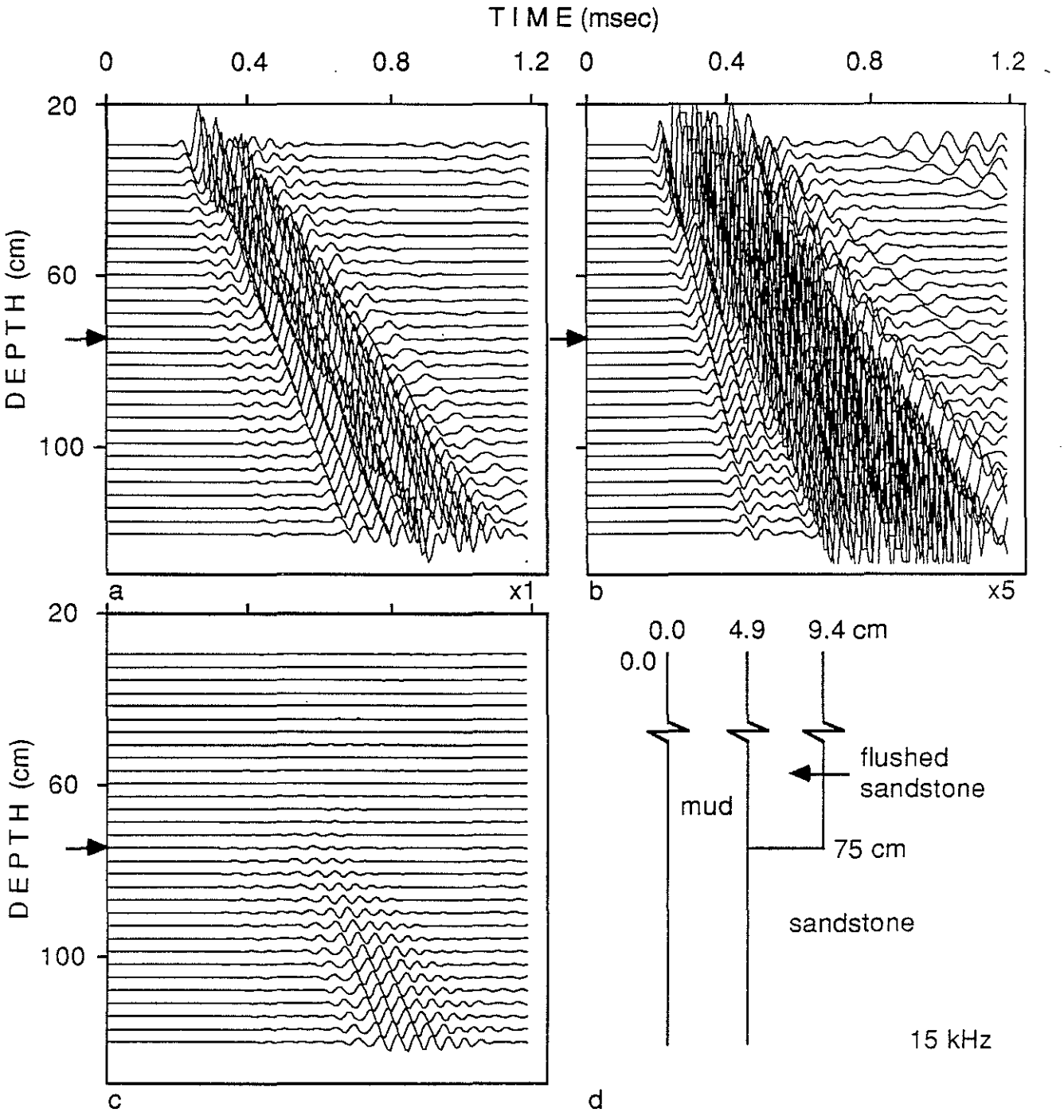

Figure 12: Synthetic full waveform acoustic log for a flushed sandstone zone terminating against a sandstone.

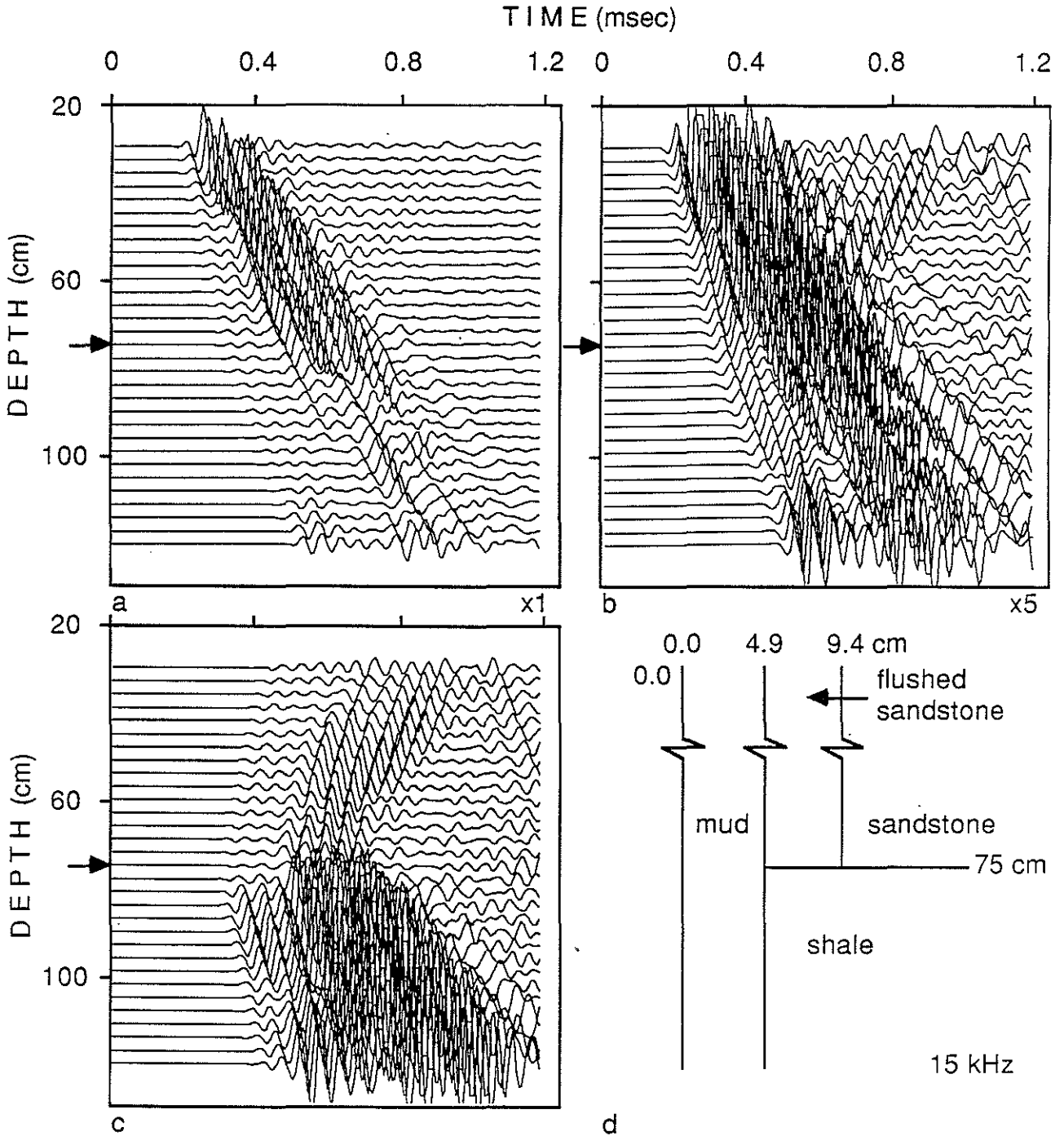

Figure 13: Synthetic full waveform acoustic log for a flushed sandstone zone terminating against a shale.

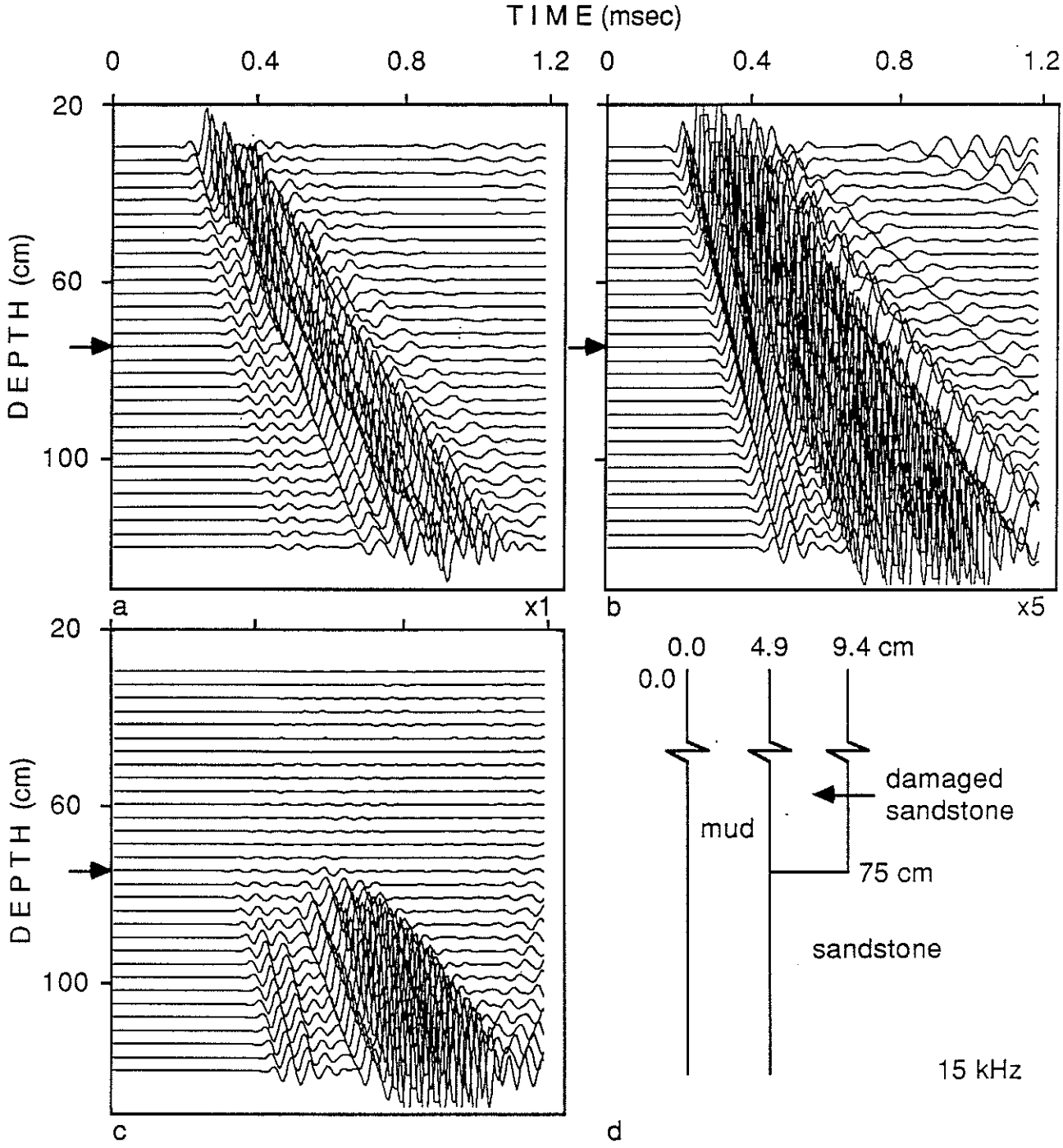

Figure 14: Synthetic full waveform acoustic log for a damaged sandstone zone terminating against a sandstone.

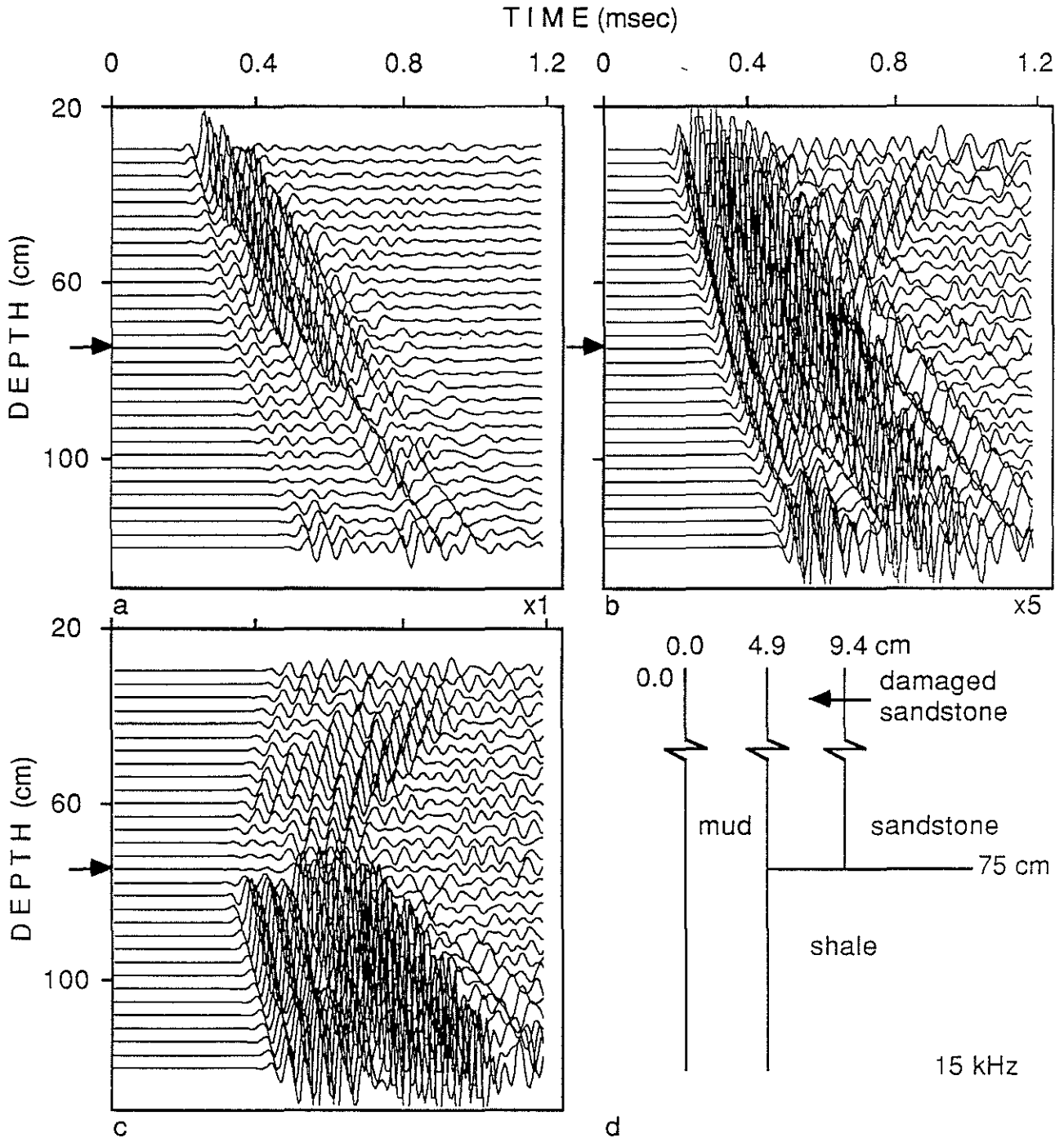

Figure 15: Synthetic full waveform acoustic log for a damaged sandstone zone terminating against a shale.

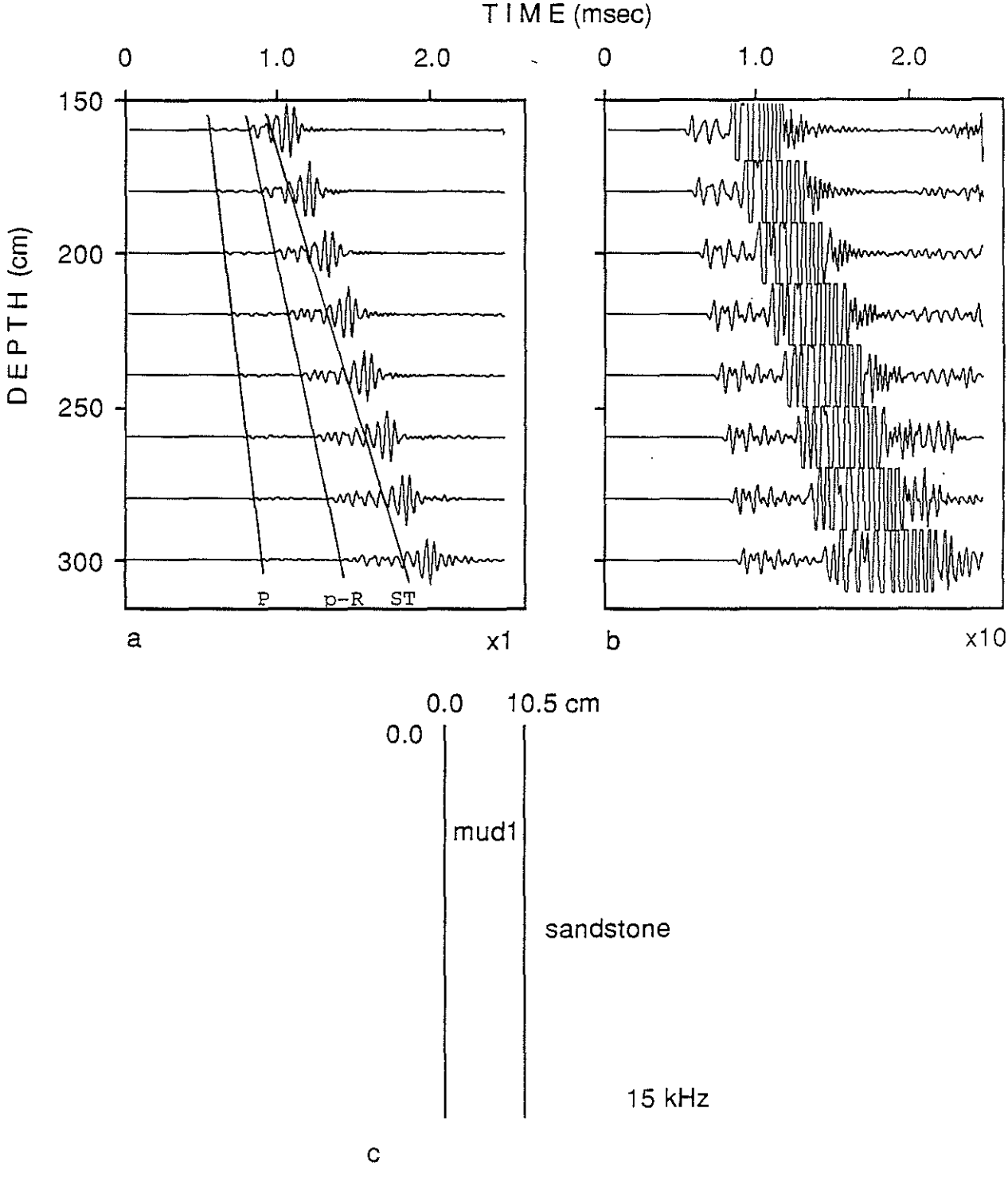

Figure 16: Synthetic full waveform acoustic log for a vertically homogeneous sandstone. Rock and mud properties and depth of receivers varies from the sandstone model of Figure 1.

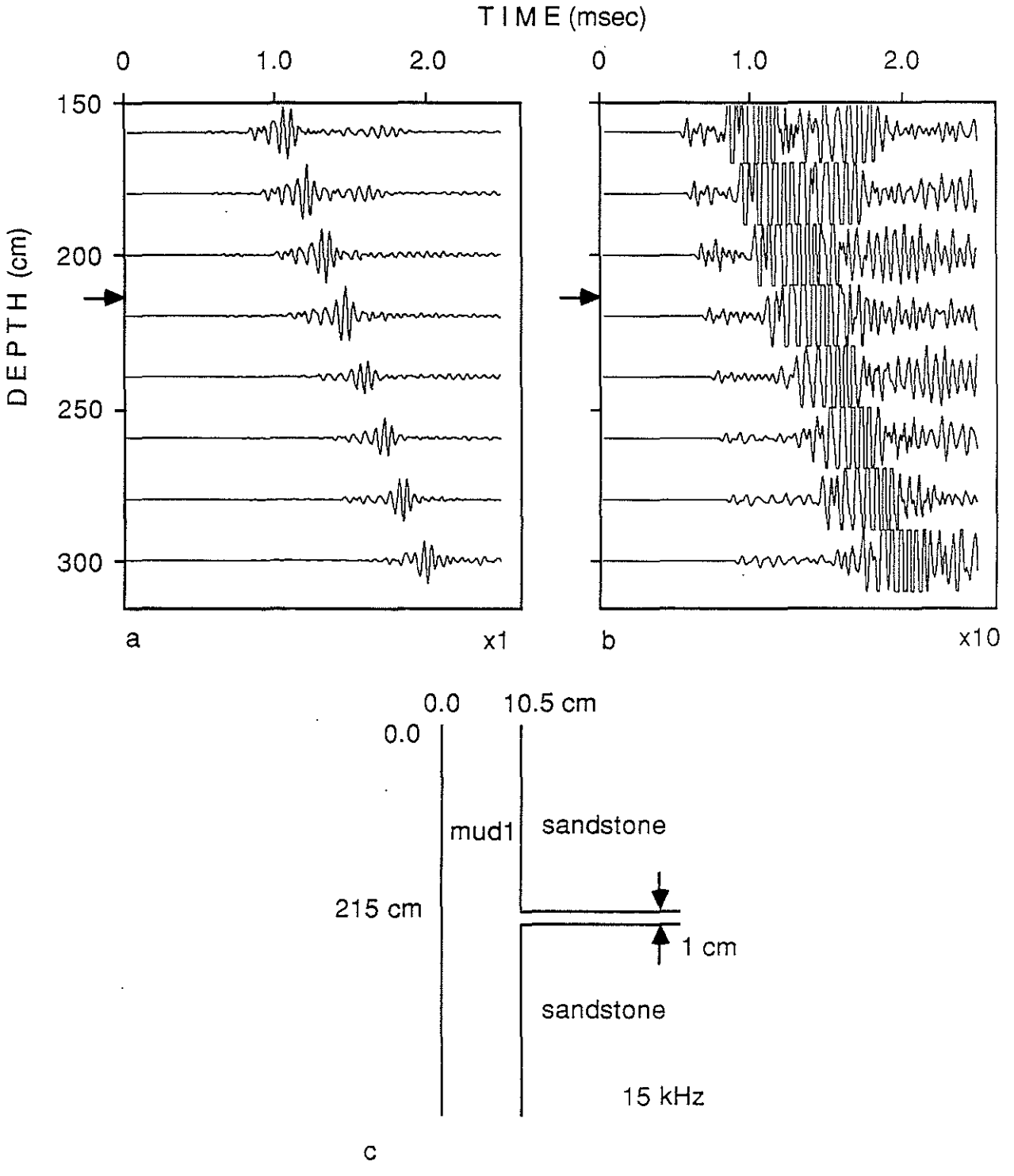

Figure 17: Synthetic full waveform acoustic log for a 1 cm thick horizontal fissure.

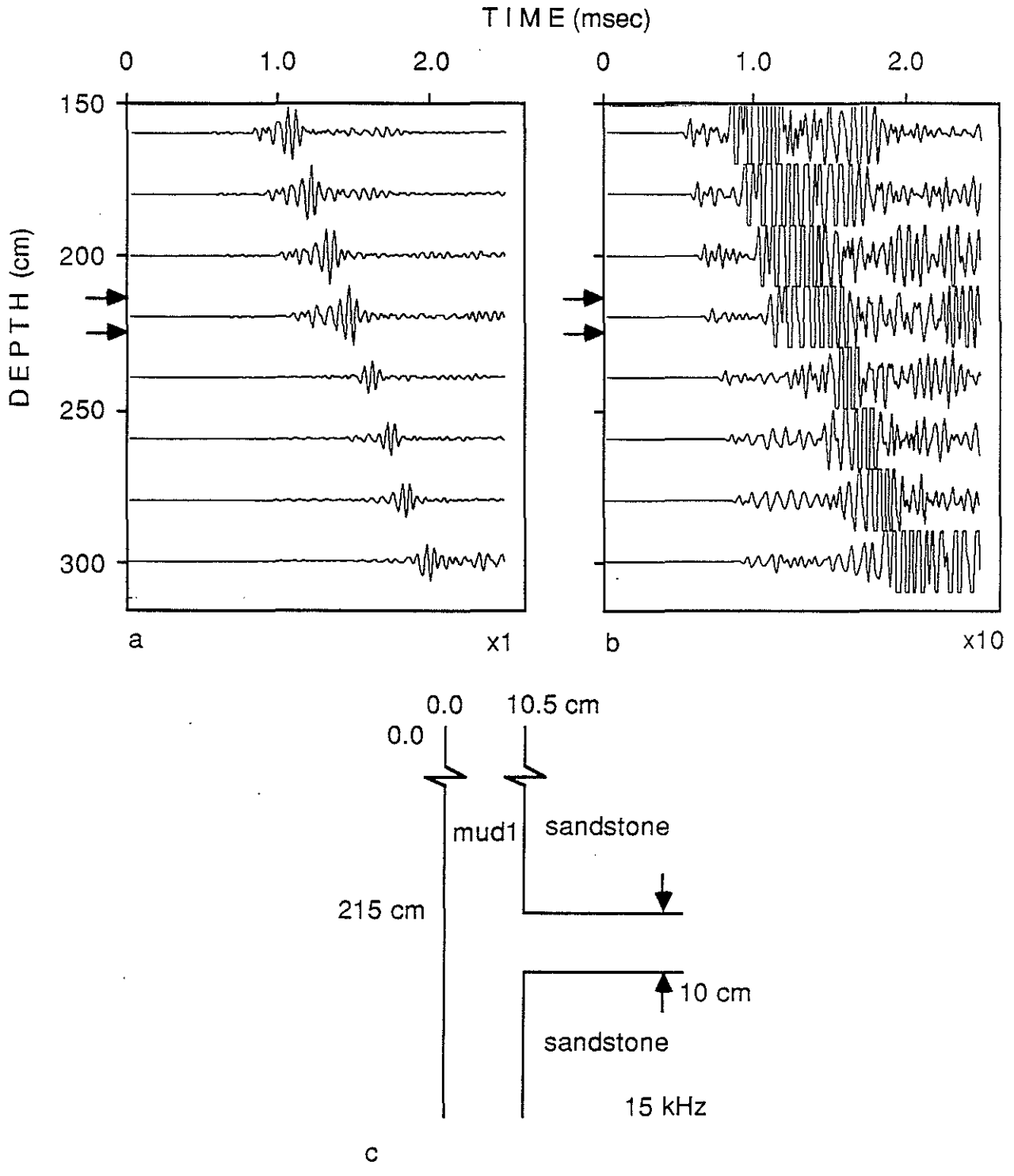

Figure 18: Synthetic full waveform acoustic log for a 10 cm thick horizontal fissure.

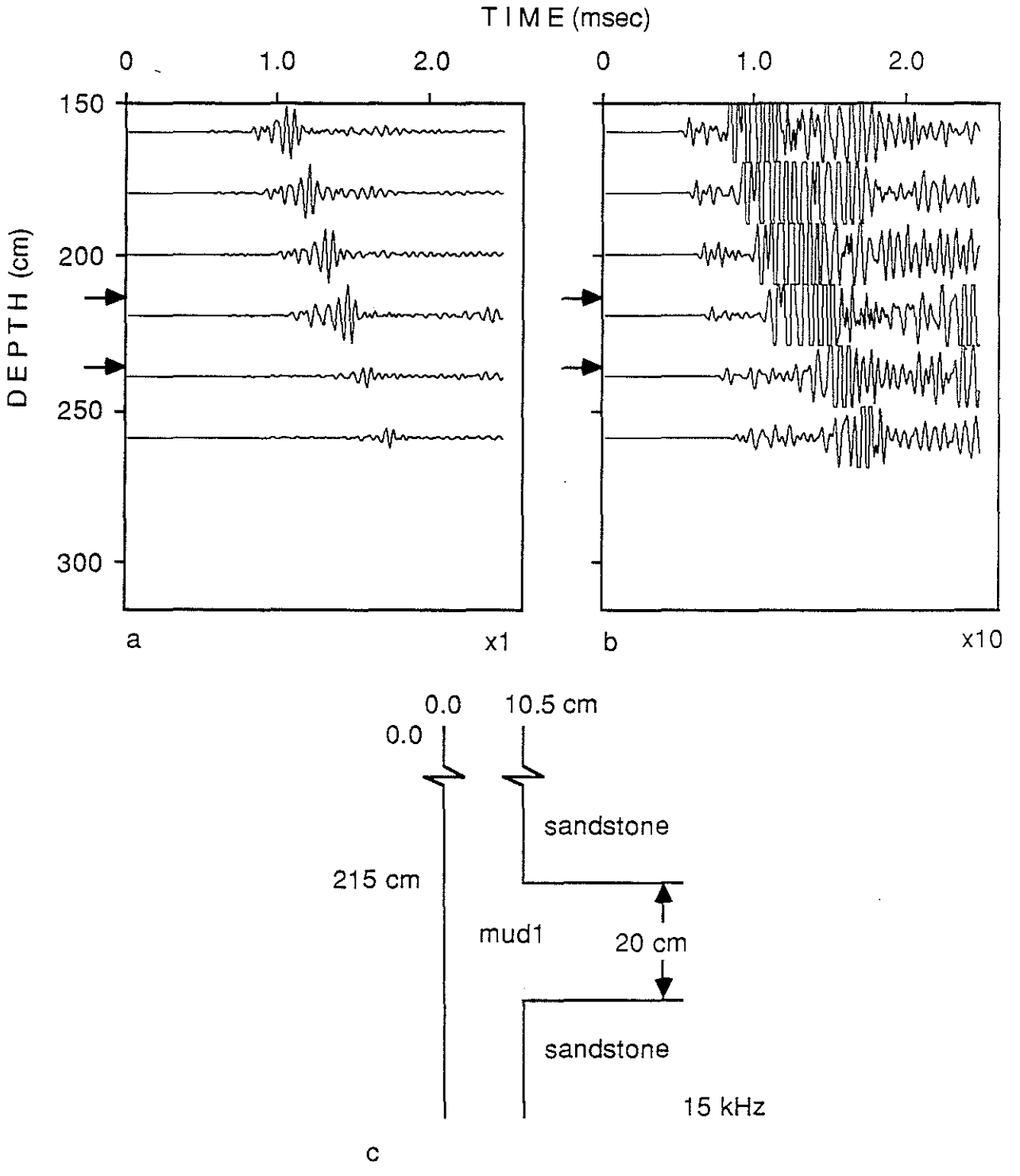

Figure 19: Synthetic full waveform acoustic log for a 20 cm thick horizontal fissure.

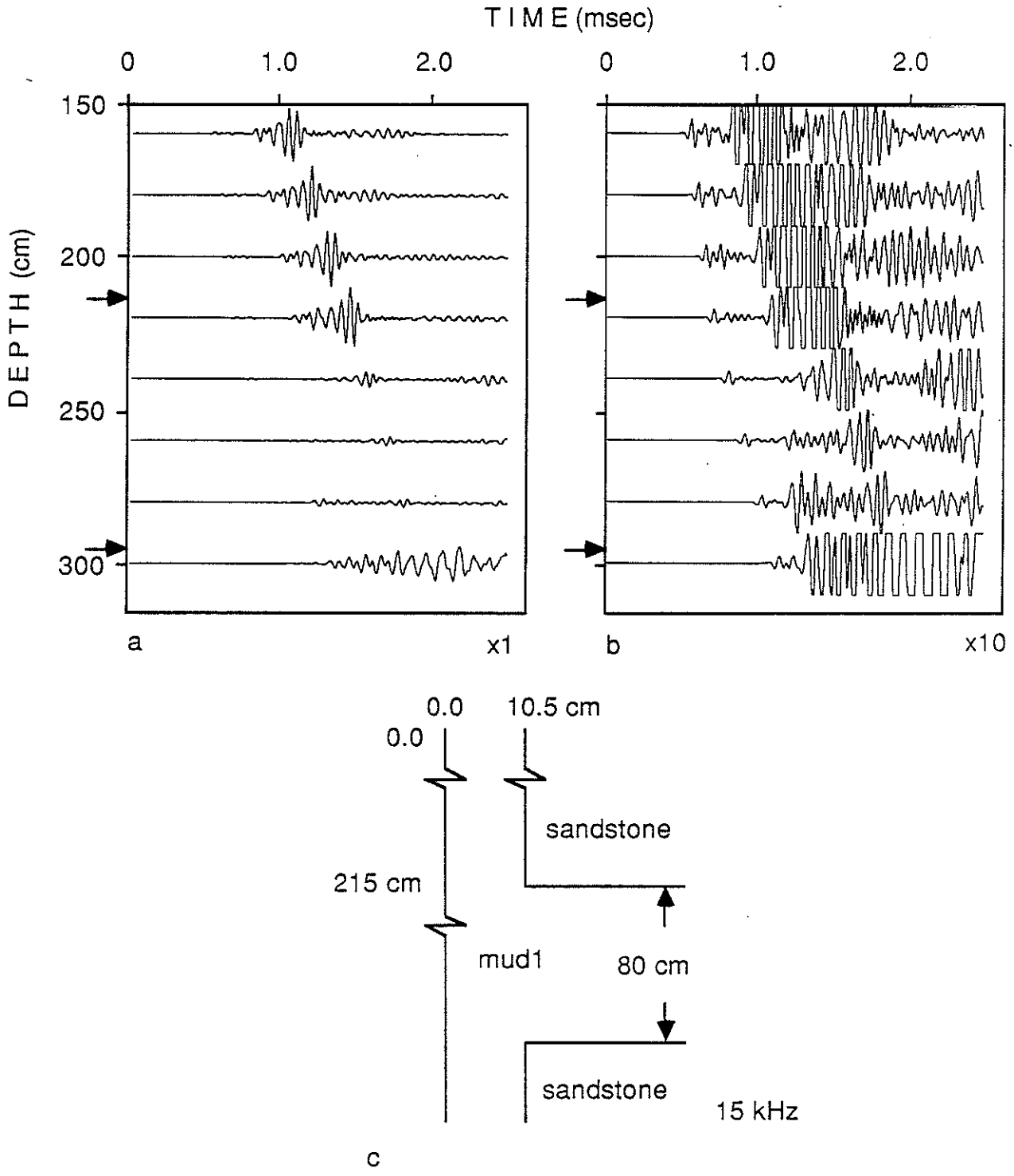

Figure 20: Synthetic full waveform acoustic log for a 80 cm thick horizontal fissure.

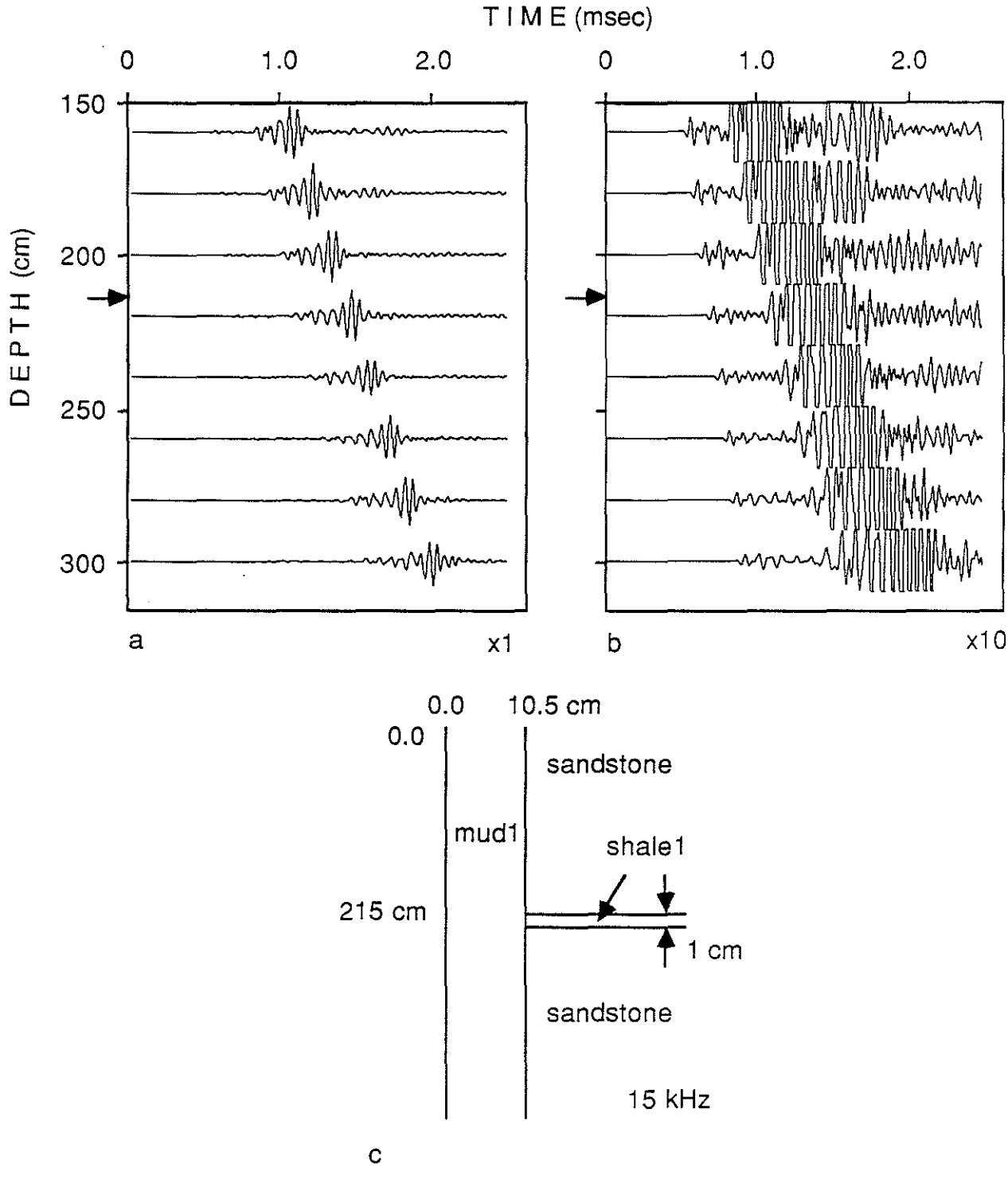

Figure 21: Synthetic full waveform acoustic log for a 1 cm thick horizontal shale stringer.

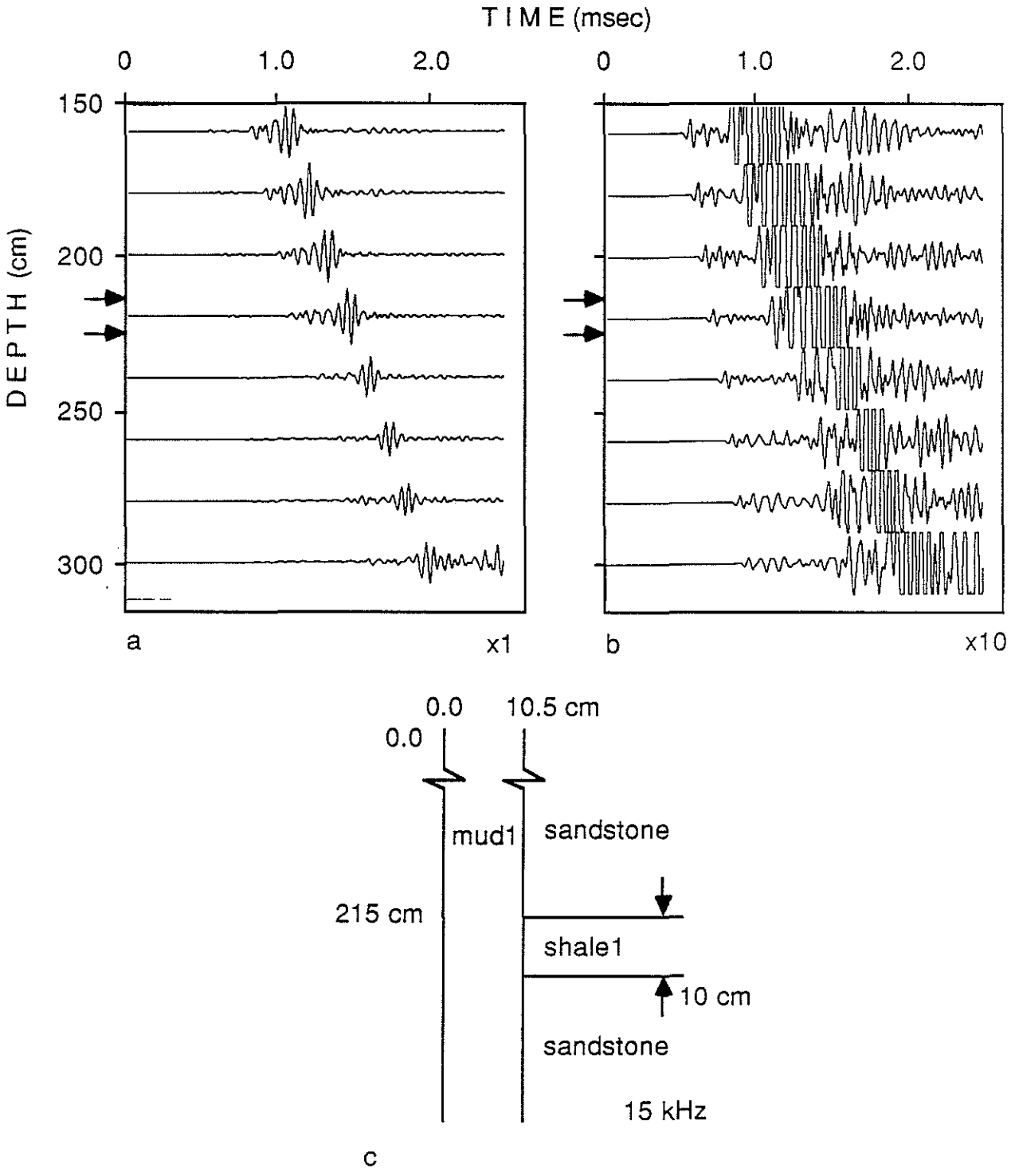

Figure 22: Synthetic full waveform acoustic log for a 10 cm thick horizontal shale stringer.

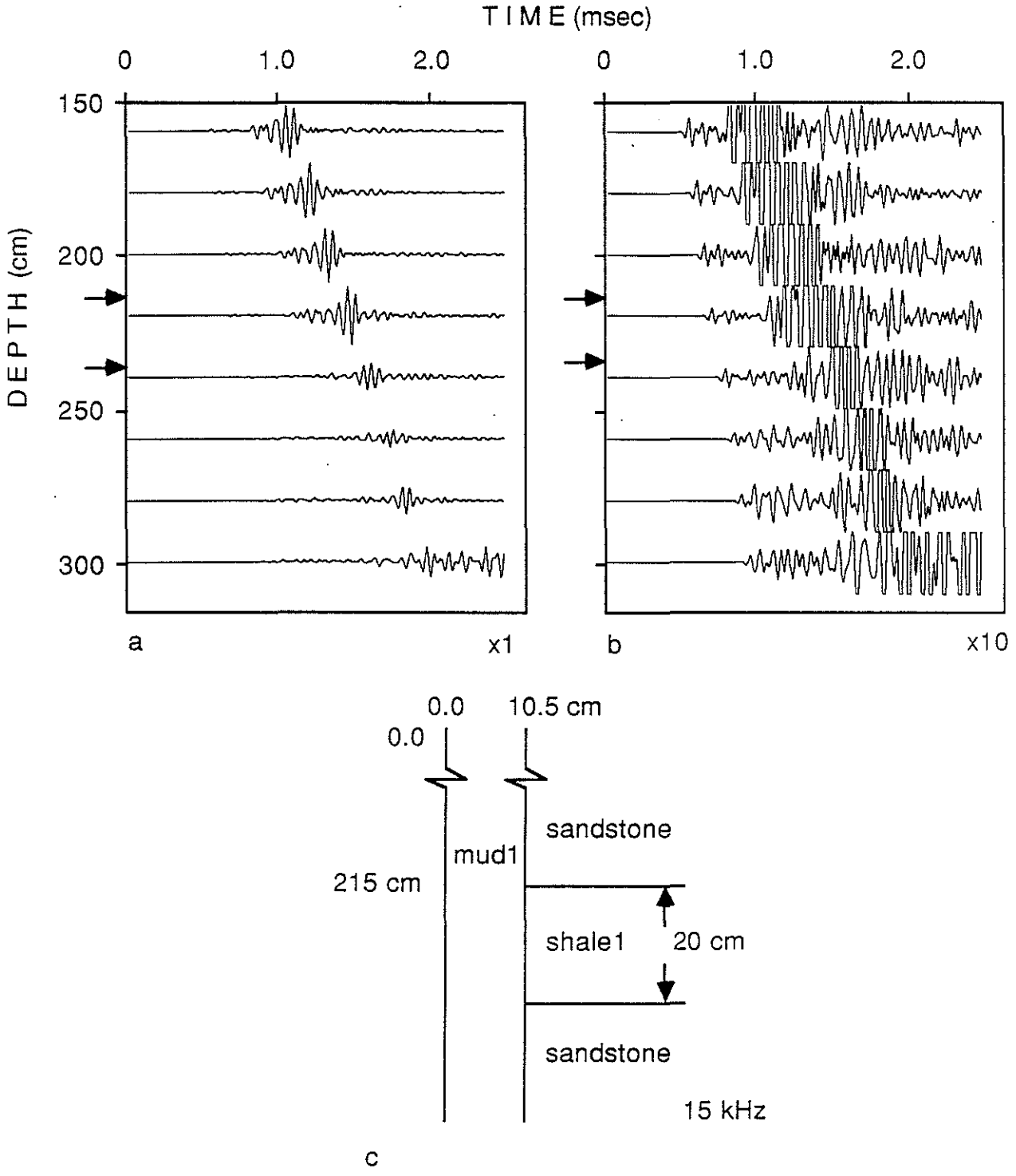

Figure 23: Synthetic full waveform acoustic log for a 20 cm thick horizontal shale stringer.

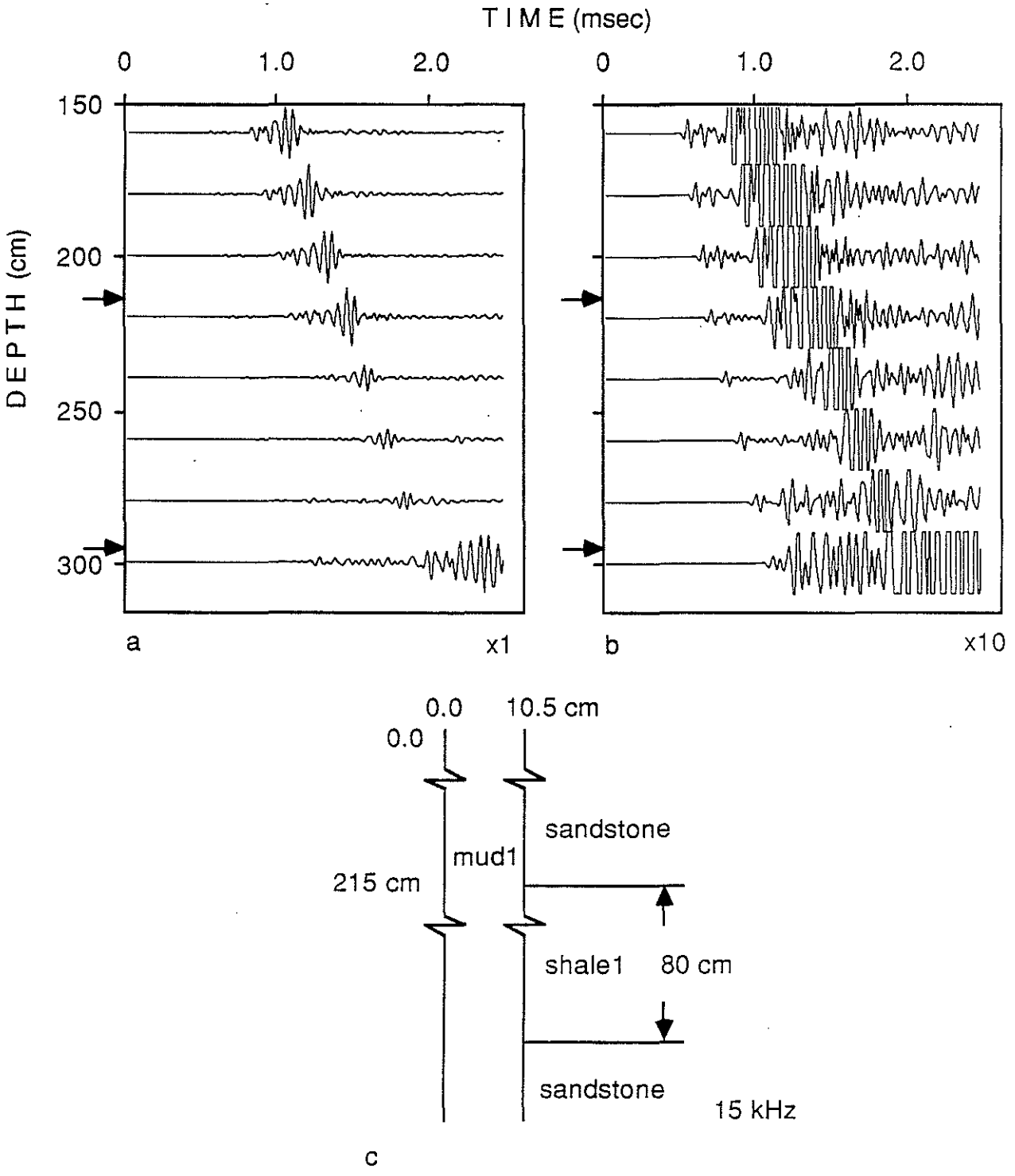

Figure 24: Synthetic full waveform acoustic log for a 80 cm thick horizontal shale stringer.

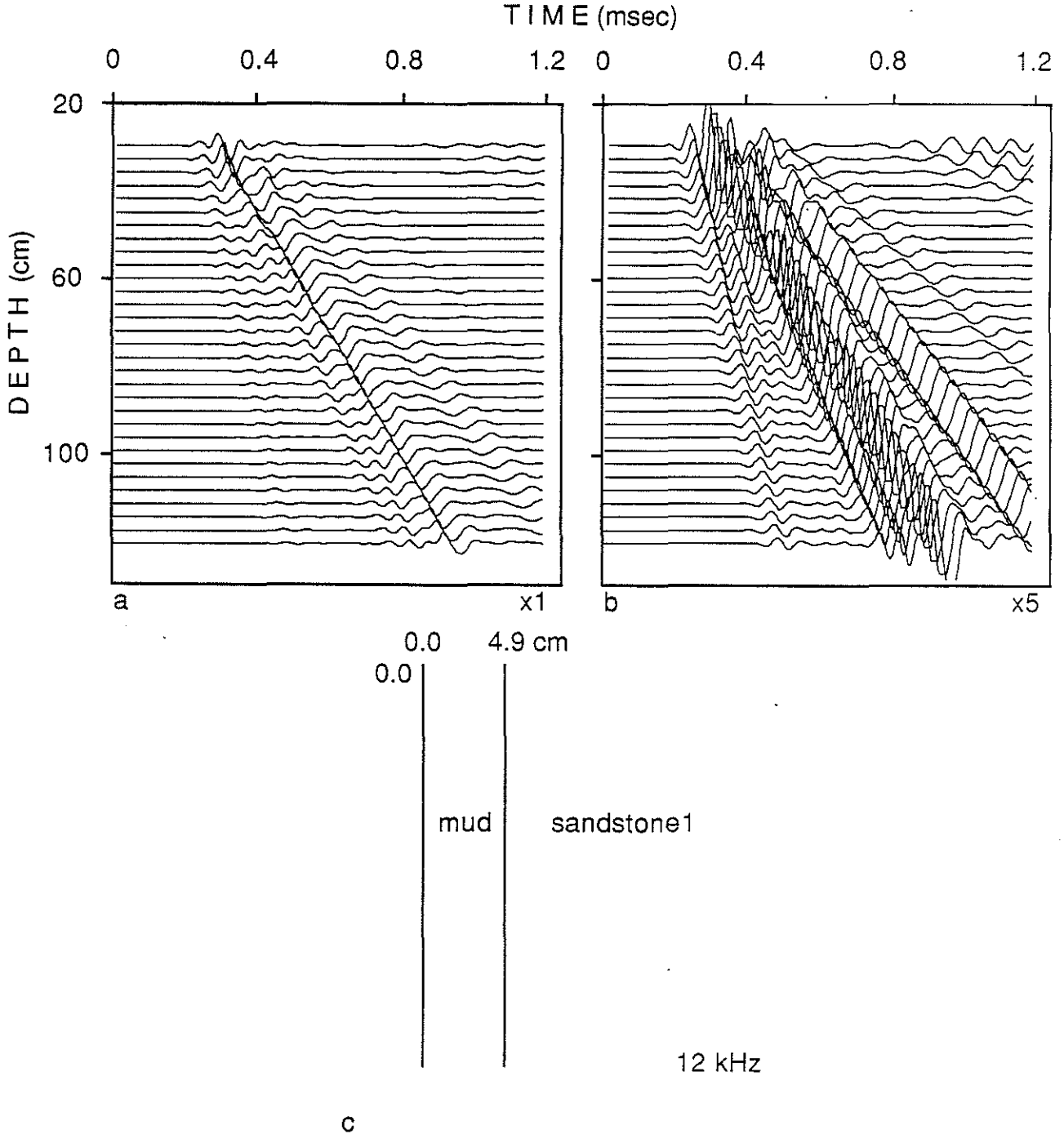

Figure 25: Synthetic full waveform acoustic log for a vertically homogeneous sandstone model. Formation shear wave velocity and source frequency differ from the models in Figures 1 and 16.

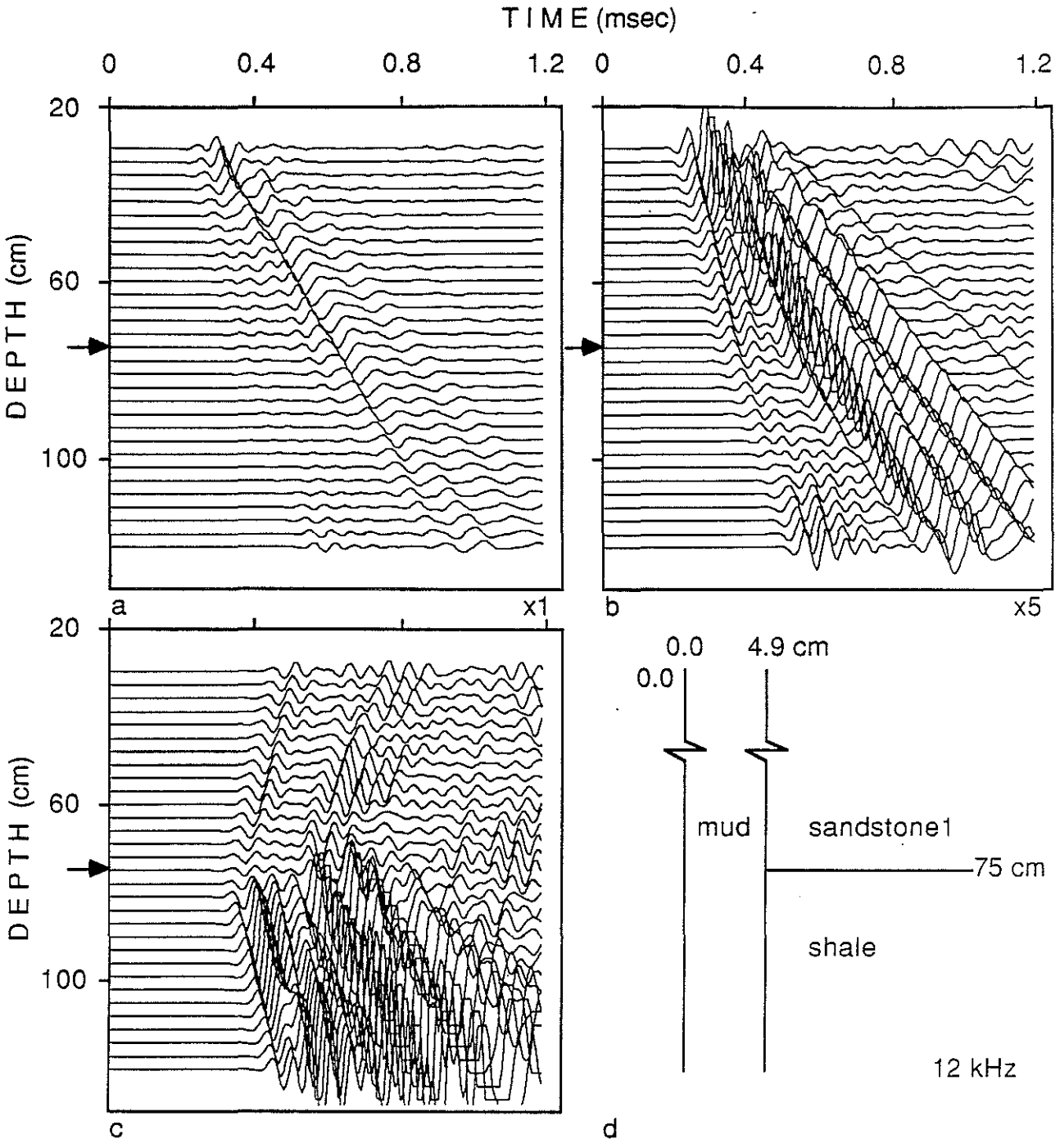

Figure 26: Synthetic full waveform acoustic log for a sandstone-shale contact.

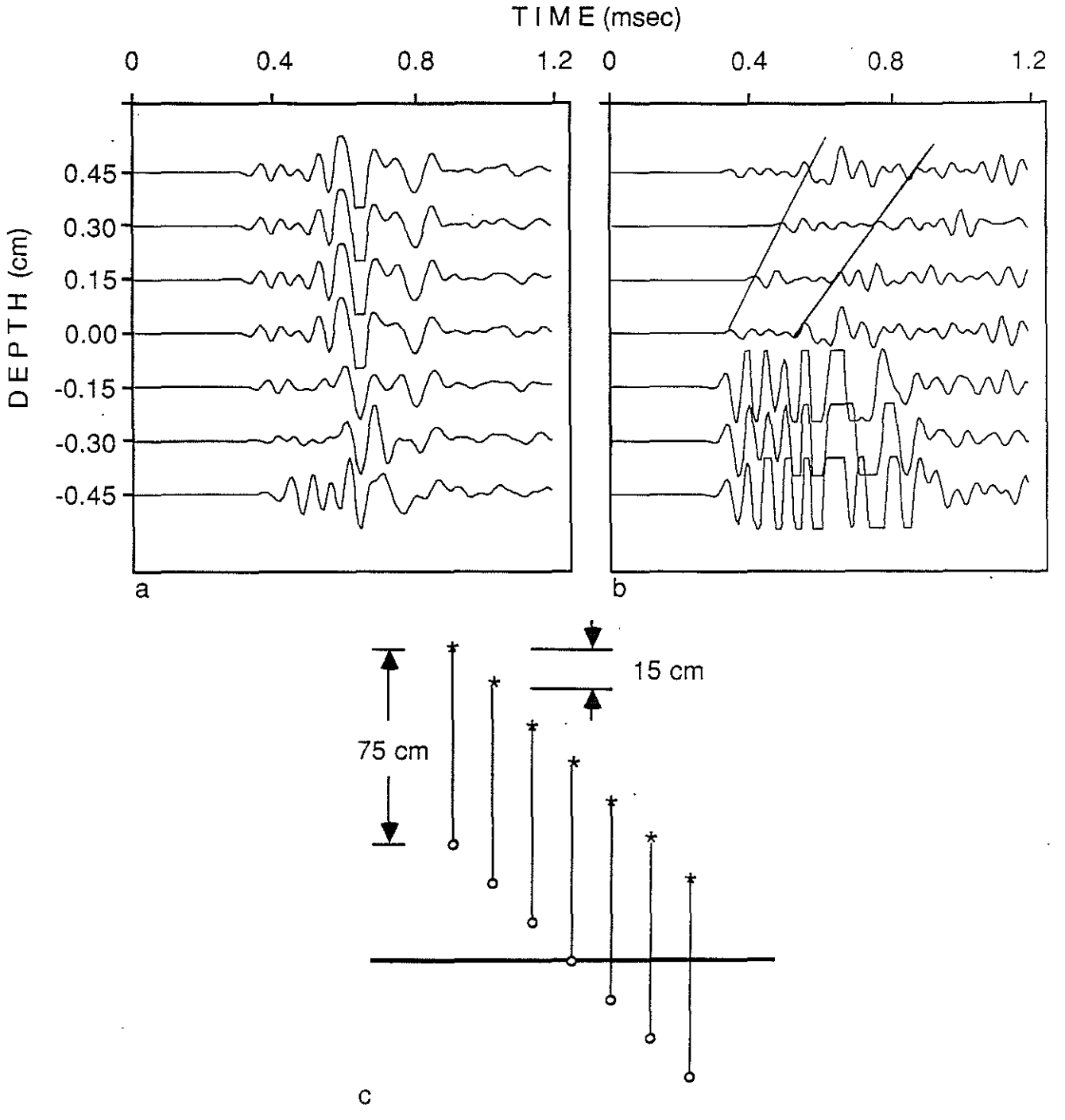

Figure 27: An actual log run past a sandstone-shale contact. Source-receiver separation is 75 cm and the interval between source locations is 15 cm.

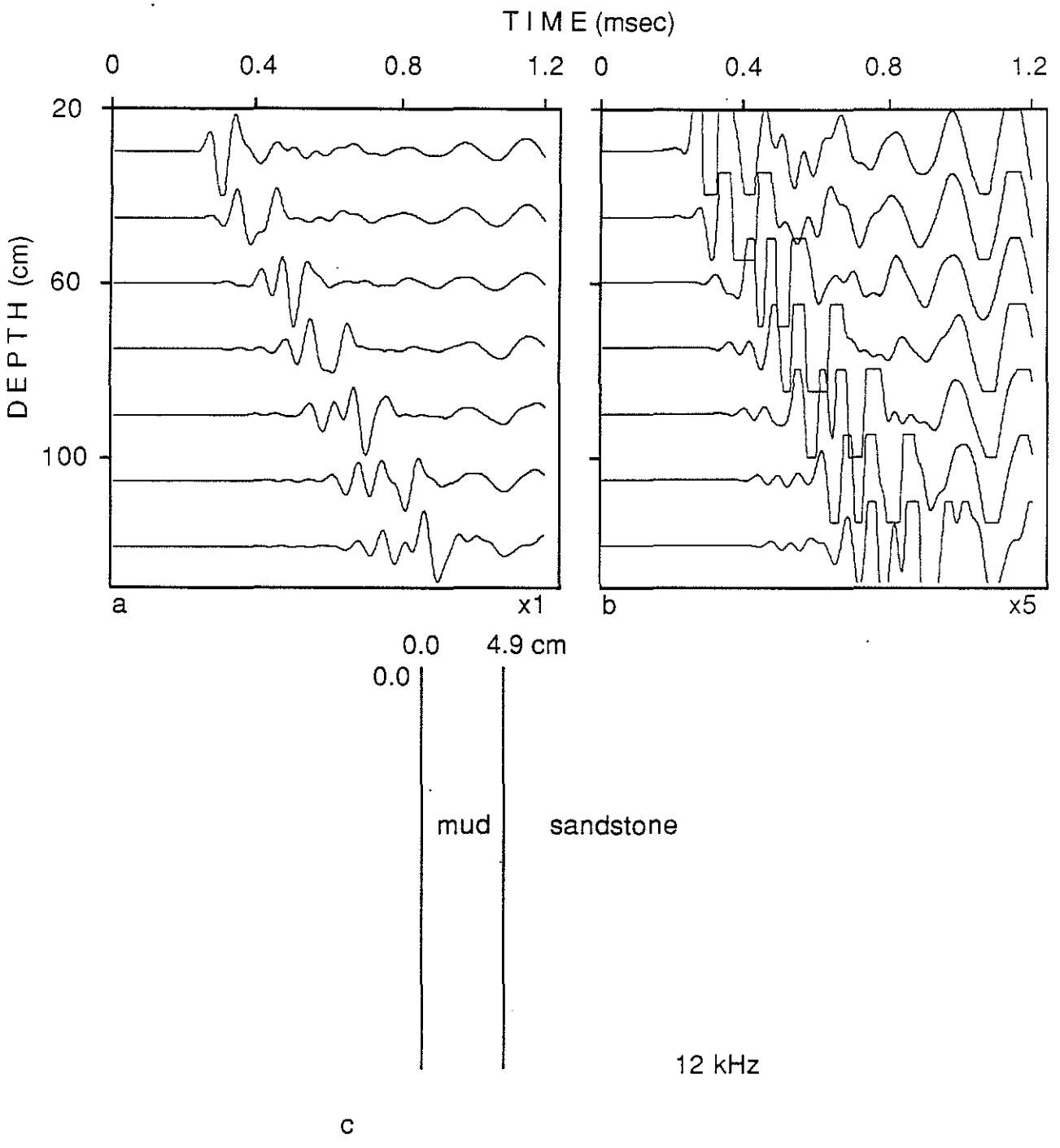

Figure A-1: A synthetic acoustic log in a uniform sandstone (as Figure 1) with a 12 kHz source. The source time dependence and the model are identical to Figure 4-1 of Bhasavanija (1983). However Bhasavanija introduces the source as a distribution of horizontal displacements only. In this figure the source was introduced as a distribution of compressional point sources and is more physically correct. The differences are primarily in the pseudo-Rayleigh wave packet.

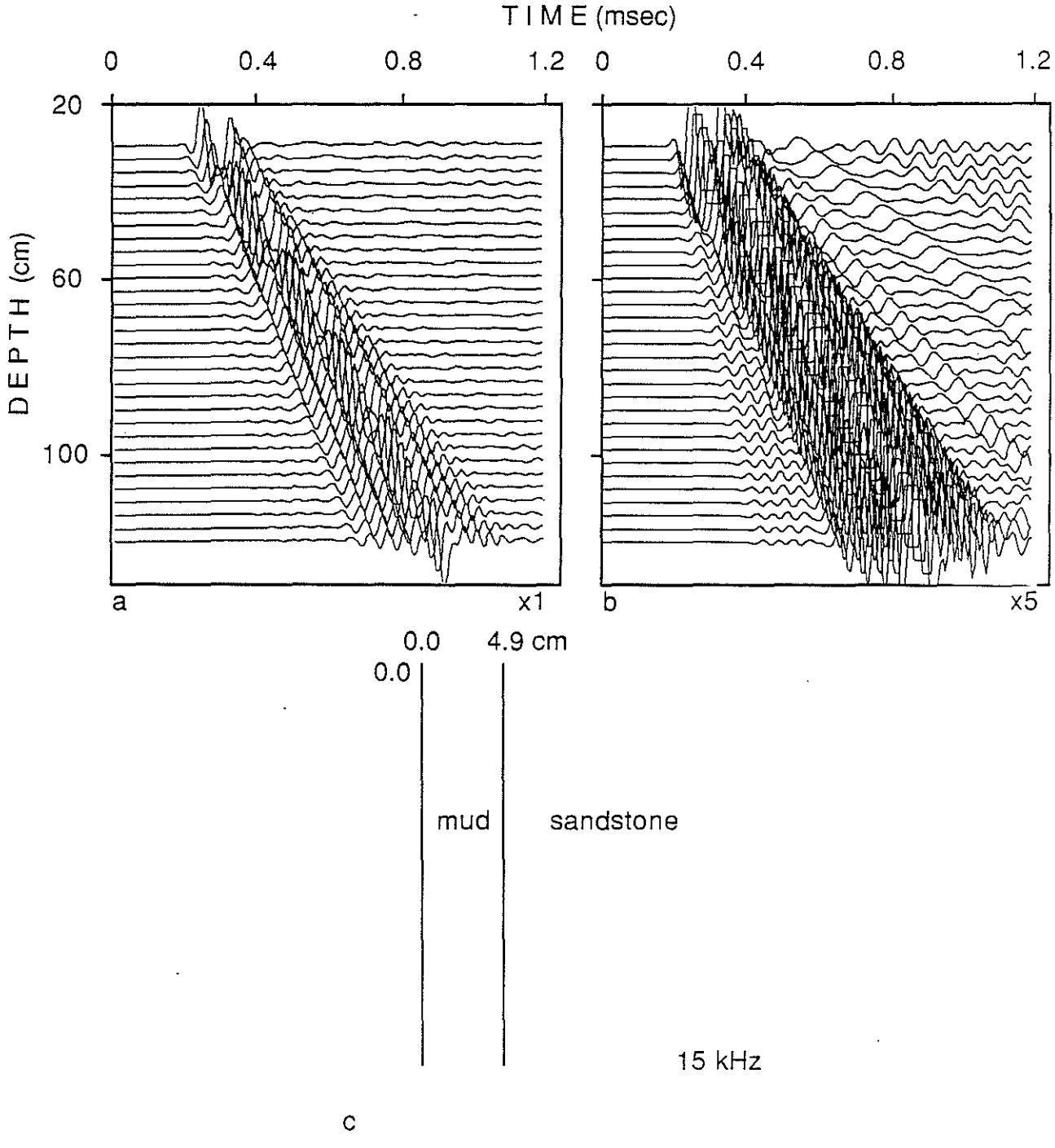

Figure A-2: A synthetic acoustic log in a uniform sandstone at 15 kHz. The source is a compressional point source and no tool is considered.

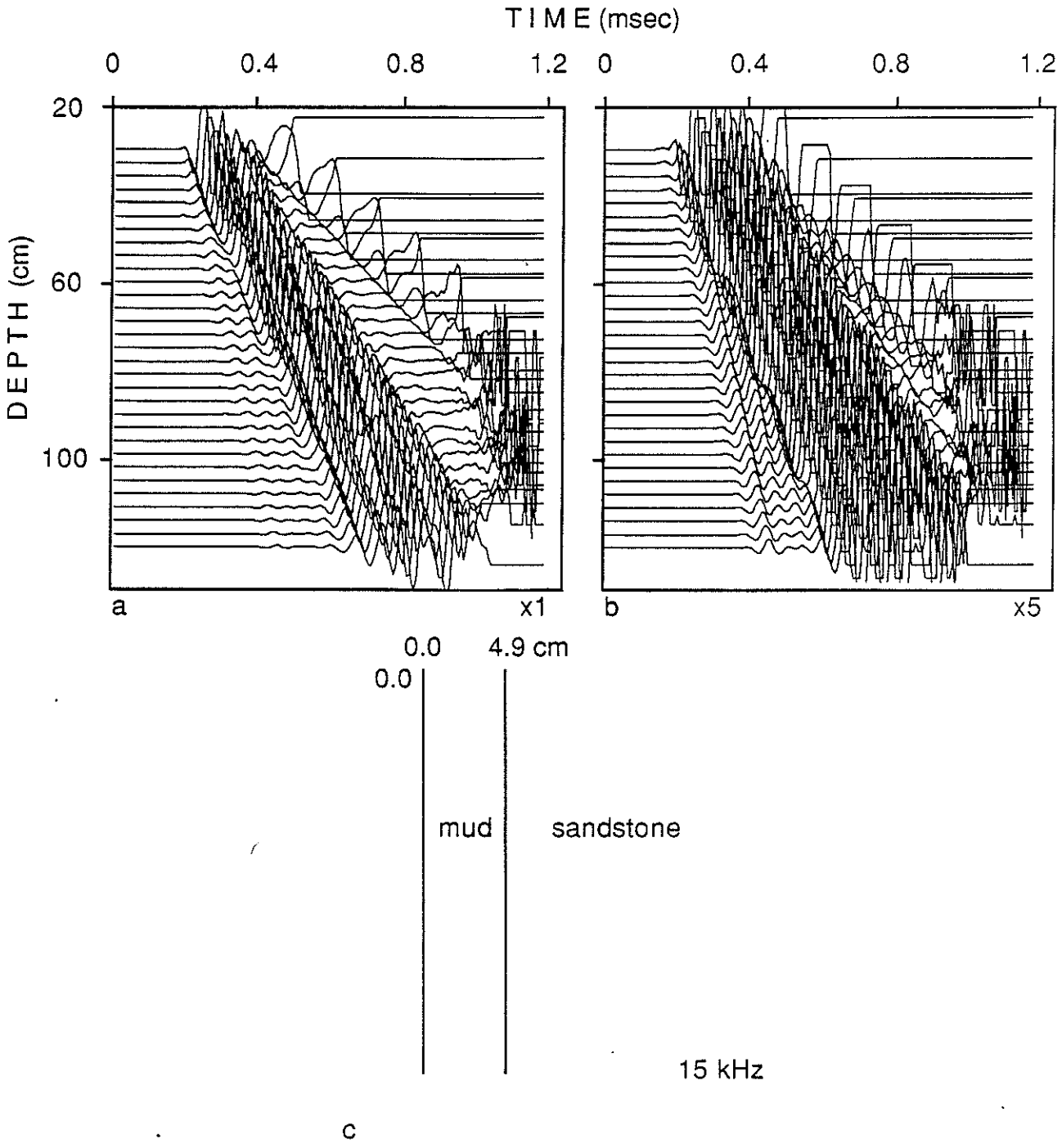

Figure A-3: A synthetic acoustic log in a uniform sandstone at 15 kHz. The source is a distribution of compressional point sources over 10 cm and a tool is introduced as described in the text.

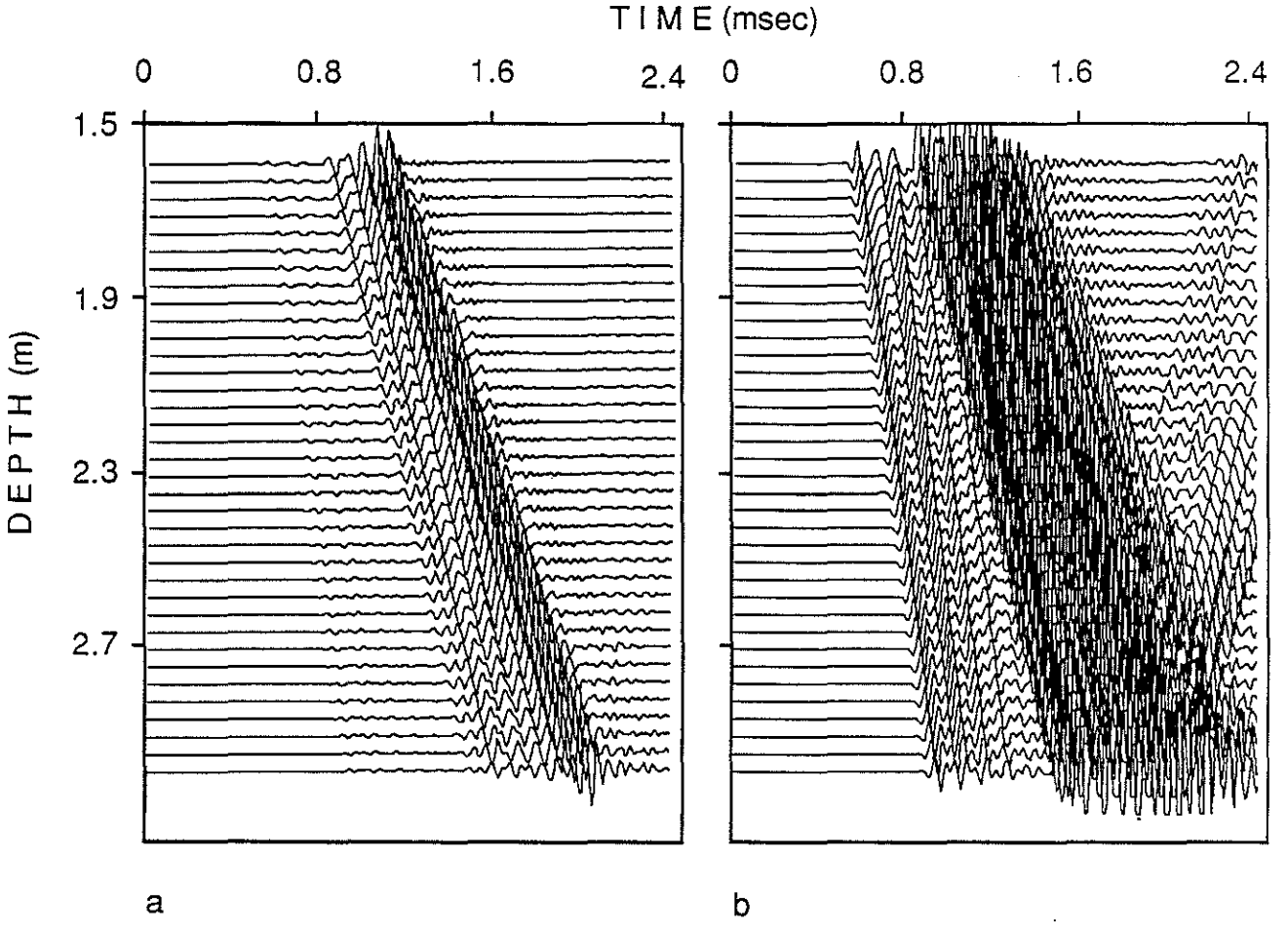

Figure B-1: The time-space representation of an acoustic log in a uniform sandstone at 15 kHz which is used for the two dimensional Fourier transform study. Note the presence of compressional head waves, PL modes, pseudo-Rayleigh waves, and Stoneley waves.

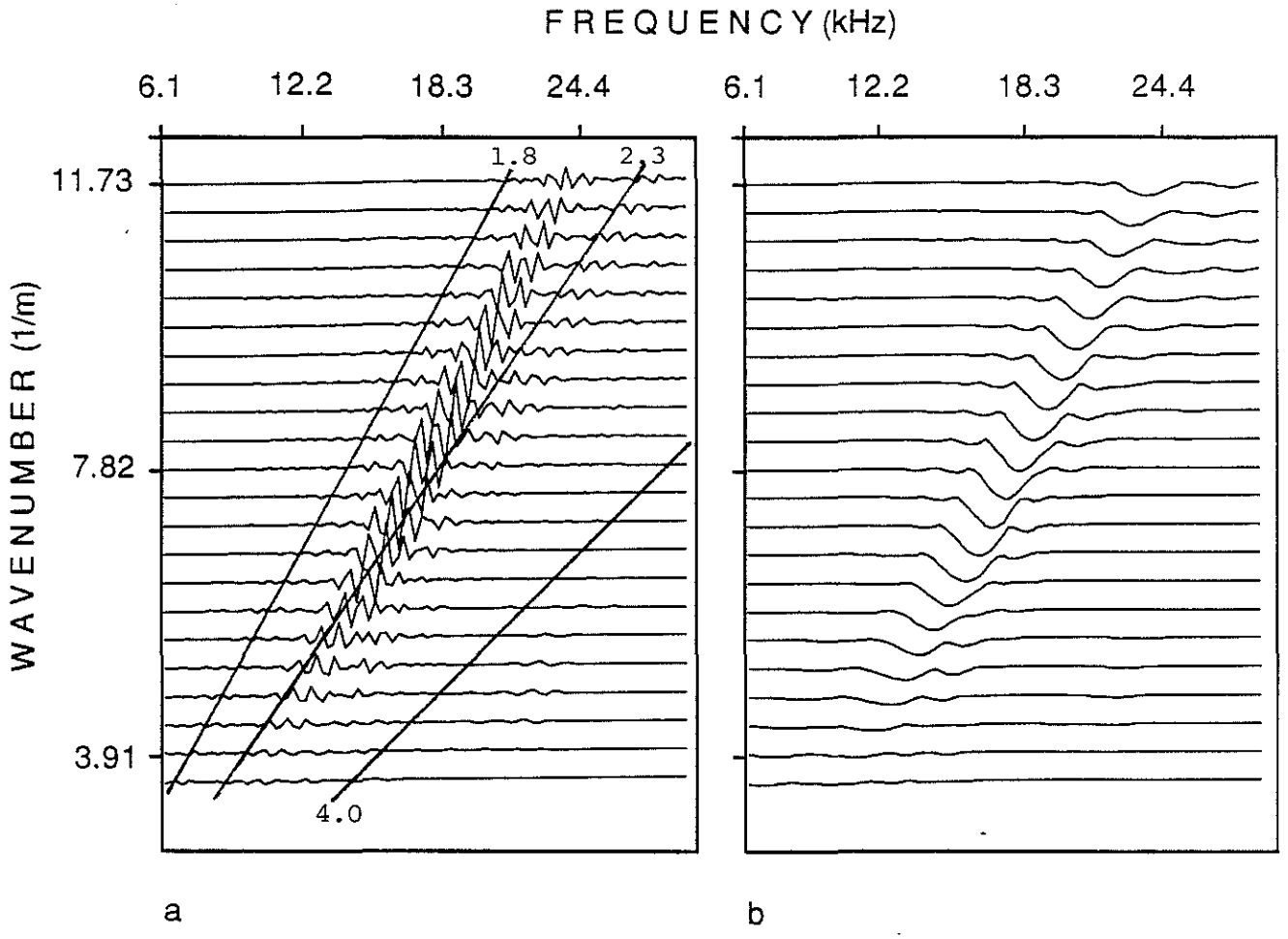

Figure B-2: The frequency-wavenumber representation of the time series in Figure B-1. Figure B-2a is the real part of the spectra and Figure B-2b is the power spectrum.

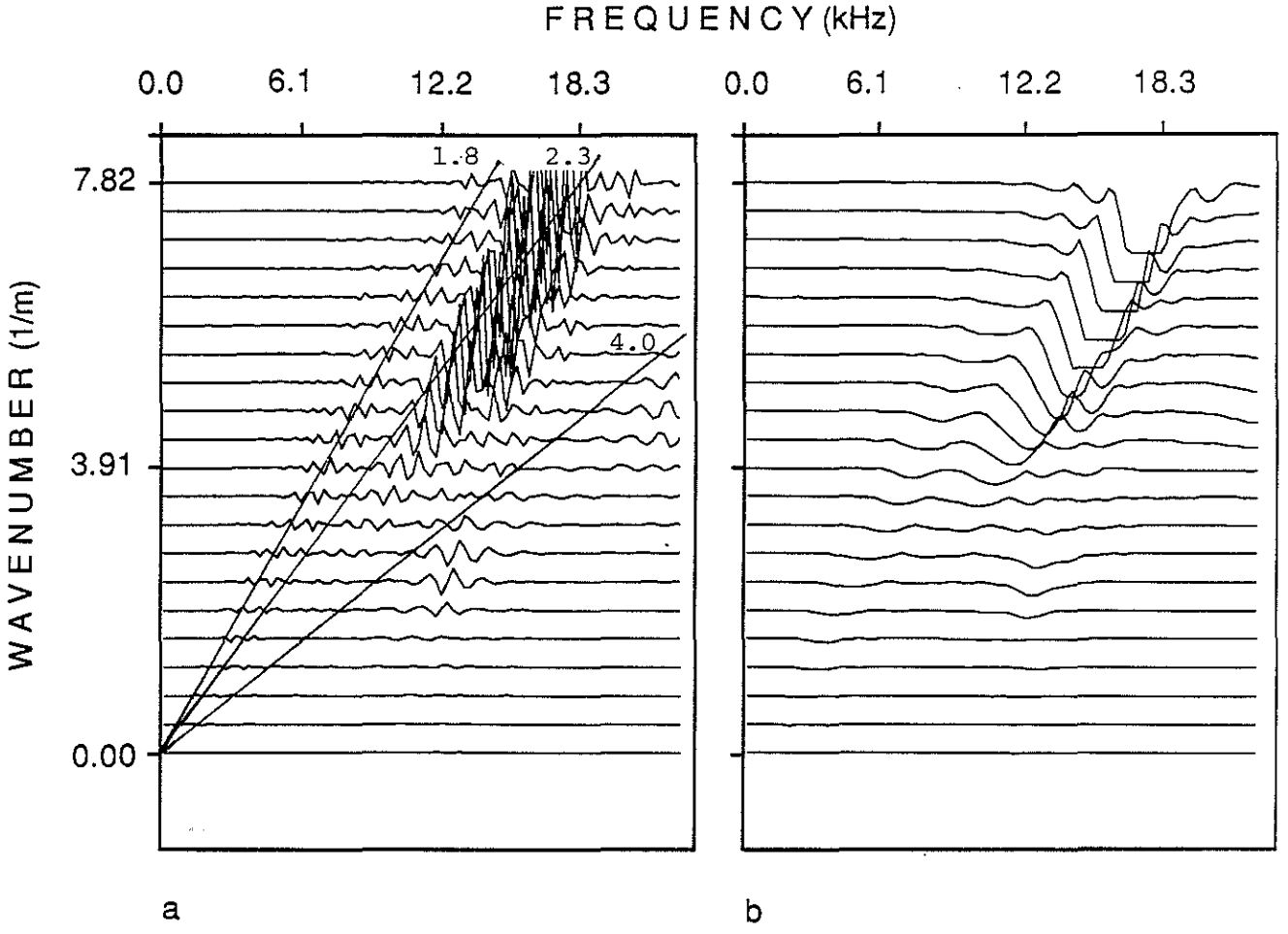

Figure B-3: A different section of the frequency-wavenumber domain shown in Figure B-2.